Spring 4-15-2021

Development of a Low-cost Efficient Wireless Intelligent Sensor for Strain (LEWIS-S) and Applications in Measuring Nonlinear Dynamics

Eric Robbins

Eric Robbins

Candidate

Civil, Construction, and Environmental Engineering

Department

This thesis is approved, and it is acceptable in quality and form for publication:

Approved by the Thesis Committee:

Fernando Moreu, Chair

Rafiqul Tarefder

Robert Kuether

Development of a Low-cost Efficient Wireless Intelligent Sensor for Strain (LEWIS-S) and Applications in Measuring Nonlinear Dynamics

by

Eric Robbins

B.S., Civil Engineering

University of New Mexico, NM, 2019

A thesis submitted in partial fulfillment of the requirements for the degree of

MASTER OF SCIENCE

IN

CIVIL ENGINEERING

Department of Civil, Construction, and Environmental Engineering

University of New Mexico

Albuquerque, New Mexico

May 2021

Dedication

I dedicate this thesis to my friends and family, who have helped me overcome the various challenges I faced throughout this research. Specifically, I would like to thank my parents Mark and Jeanne for teaching me the invaluable lessons of hard work and studying. I would also like to thank my brother Aron for his support throughout my research.

Acknowledgements

I want to thank my advisor and committee chair Dr. Fernando Moreu for his strong support and endless help throughout this research. I would also like to thank Dr. Robert Kuether, and Dr. Rafiqul Tarefder for accepting positions on my defense committee. Thank you, Dr. Robert Kuether and Benjamin Pacini for all the help throughout this research. Lastly, I would like to thank the various members and my fellow colleagues at the Smart Management of Infrastructure Laboratory for their continuous help and support.

Development of a Low-cost Efficient Wireless Intelligent Sensor for Strain (LEWIS-S) and Applications in Measuring Nonlinear Dynamics

by

Eric Robbins

B.S., Civil Engineering, University of New Mexico, NM, 2019

M.S., Civil Engineering, University of New Mexico, NM, 2021

Abstract

Nonlinearities exist in all real-life systems and can be caused by behaviours such as large deformations, yielding, contact, etc. which can result in phenomena not found in linear testing. Considering nonlinear behaviour in dynamic analyses can be beneficial to increase model predictability and can accurately characterize system responses. Generally, accelerometers are commonly used in linear and nonlinear vibration testing to obtain the acceleration response of a system. However, some systems may render the use of accelerometers problematic, or accelerometers may introduce limitations to measurement capabilities such that it can be beneficial to obtain experimental data using different sensors. In the context of experimental data, strain gauges can alternatively be used to obtain dynamic properties both in the laboratory and in the field. Strain gauges are additionally capable of quantifying damage that is directly estimated from strain measurements, such as stresses, that accelerometers cannot obtain. But, measuring strain in structural dynamics can be disincentivizing and expensive due to the complexity of data acquisition, lack of portability, high costs, and the requirement of prior knowledge and training required for a proper installation. The purpose of this research is to introduce an alternative resource to measure nonlinear dynamics of structures using strain in a cost-effective and streamlined platform. This thesis accomplishes the goal of developing and testing a low-cost, efficient, wireless, intelligent sensor for strain (LEWIS-S) for the nonlinear

dynamic assessment of a simple structure. The LEWIS-S sensor functions on a platform of various Arduino hardware components and free Integrate Development Environment (IDE) software. Two different sensor configurations were used in the validation testing in this research, namely, a uniaxial friction-magnetic strain checker and a traditional pasted uniaxial strain gauge. Static and dynamic validation tests were conducted on a small cantilever beam where the LEWIS-S was compared to a commercial DAQ system to verify the accuracy and dependability of the sensor. The LEWIS-S sensor was then used in nonlinear dynamics tests to experimentally characterize the softening behaviour of a cantilever beam with geometric and inertial nonlinearities produced by large deformations. Two experiments were performed on a nonlinear cantilever beam with measurements obtained at the base with the LEWIS-S sensor and at the tip using an accelerometer. The first test was a sine sweep through the fundamental resonance of the system and the second test was a ring-down from an initial static deformation. Based on the results of the validation and nonlinear experimental testing, the LEWIS-S sensor demonstrated various streamlined sensing capabilities. Namely, the sensor is approximately 95% cheaper than standard commercial equipment and the compact design reduces the plan-view-footprint of the equipment by approximately 75%. Furthermore, the small footprint and wireless function enhances the portability which increase sensing capabilities. The versatility of the sensor also allows for the compatibility of different strain gauge attachments which can be useful for sensing optimization during testing. Additionally, the LEWIS-S has an inherently simple design such that limited knowledge is required to manually assemble and use the sensor. Future research proposes deploying the LEWIS-S in field testing as well as advancing the performance of the LEWIS-S by addressing sensor limitations.

Table of Contents

List of Figures

List of Tables

Chapter 1 Introduction

This research summarizes the development, design, validation testing, and laboratory experimentation of the low-cost, efficient, wireless, intelligent sensor for strain (LEWIS-S). The contribution of this research decreases costs and size and increases efficiency, portability, and versatility of strain sensing, while maintaining a simple design that requires limited knowledge to assemble. The focus of this work is directed to the design and validation testing of the LEWIS-S sensor in static and dynamic testing compared to commercial DAQ equipment. Additionally, this research also focuses on the application of the LEWIS-S in a nonlinear dynamics test to compare the responses of the LEWIS-S sensor to an accelerometer for measuring large displacements on a cantilever beam. The following section introduces the importance of nonlinear experimental dynamics, structural health monitoring (SHM) sensors, and the strain sensing.

1.1 Nonlinearity in Dynamics

Linear structural dynamic testing and analysis is widely adopted in both industry and research to characterize the dynamic behavior of structures. Because linear system theory relies on principles of superposition, invariance, and orthogonality properties, this makes analysis and test techniques particularly useful in model reduction, finite element analysis (FEA), and experimental analyses [1] which can greatly speed up analyses and decrease costs. However, these simplifications can be problematic as nonlinearities are naturally occurring in nearly all real-life systems exhibiting material, contact, or geometric nonlinear behaviors [1]. Consequently, it is important to consider nonlinear effects as it can generally increase the

accuracy and validity of an analysis [2, 3], which may be critical depending on the engineering application. More specifically, nonlinear analyses introduce new sets of phenomena that are not present in linear theory such as internal resonances, amplitude-dependent characteristics, bifurcations, or discontinuous stiffening [4]. Therefore, it is important to understand and characterize these phenomena in dynamic analyses and experiments. Figure 1 introduces a few common nonlinearities in structural dynamics.

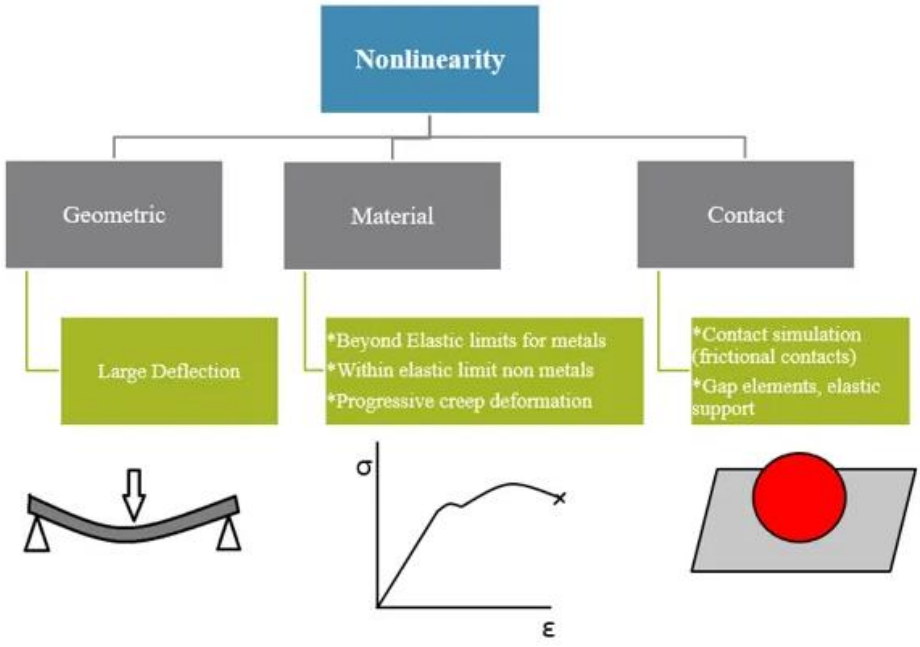

Figure 1 Three common examples of nonlinearities in structural dynamics [5]

1.2 Sensors in Structural Health Monitoring

Employing sensors in various science and engineering disciplines is critical for obtaining experimental or field measurements to make observations or quantify information about a system. Furthermore, sensors offer a broad range of diversity and relevance in experimental applications. A few topics where sensors are useful in research for example are measuring sound velocity and longitudinal viscosity of liquids [6], measuring surface strain on aircraft [7], automating train track fastener inspections [8], or measuring the response curves of soil volatile organic compounds for soil fertility [9]. Moreover, a field of research that predominantly relies on the broad use of sensor measurements is Structural Health Monitoring (SHM). To greater detail, sensors in this field are used to monitor the safety of structures and infrastructure over their lifespans. Monitoring infrastructure is of particular interest, for example, because according to the American Society of Civil Engineers (ASCE) infrastructure report card for the year of 2021, the cumulative grade for infrastructure in America was a C- [10]. In other words, infrastructure and structures are prone to damage or failure due to loading and the environment and SHM sensors can provide critical insight to help monitor and quantify safe operating conditions for structures as they age.

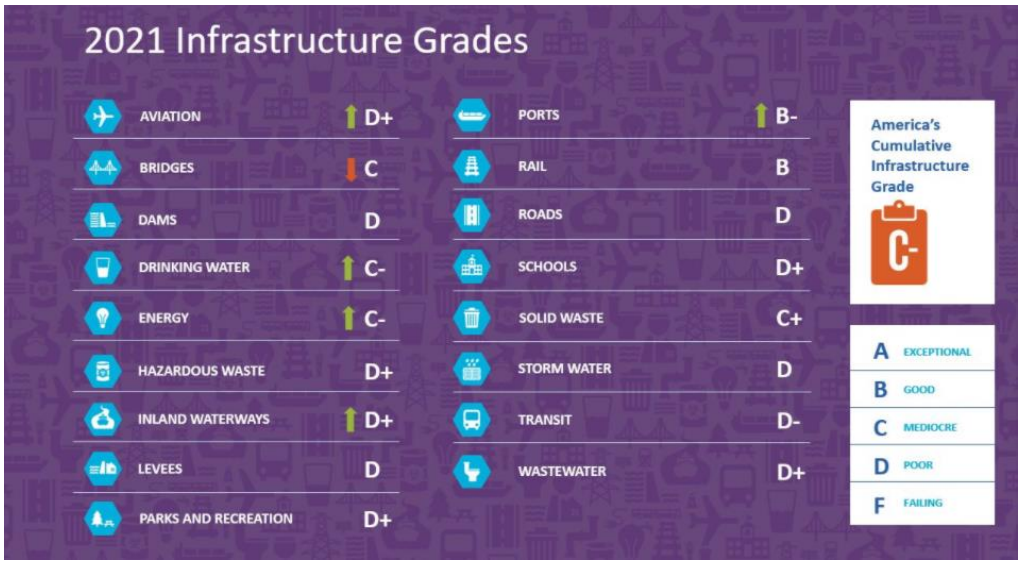

Figure 2 ASCE 2021 infrastructure grade report card [10]

1.3 Strain Sensing and Limitations

Some common structural health monitoring (SHM) measurement devices include displacement sensors (LVDT's), velocity transducers, accelerometers, and strain gauges (SG) [11]. Among the various, common monitoring sensors, measuring strain retains a particularly significant role because it can help determine important material properties such as the modulus of elasticity, yield strength, short-term fatigue, etc. which are all critical for determining damage throughout various testing [12,13]. Additionally, according to standard testing measures by ASTM, resistive strain gauges are the most widely used measurement devices for determining material properties under loads [14]. Although measuring strain offers many benefits over other types of sensing techniques, it can be very limiting and difficult to apply to test specimens as demonstrated in [15] due to the need to paste strain gauges to surfaces which is typically conducted by experienced engineers [14]. In this regard, it can be

disincentivizing to measure strain altogether. It was also shown in [15] that some common limitations of strain sensing include high costs, sensor placement and application limitations, and large DAQ systems required to take measurements which limit sensor portability.

1.4 Outline of Thesis

The LEWIS-S sensor was tested alongside traditional commercial DAQ equipment for strain measurements in both static and dynamic tests on a cantilever beam. Researchers used a traditional pasted linear resistive strain gauge and a friction-based magnetic strain gauge on the LEWIS-S and validated them against data collected on a traditional commercial DAQ system. One of the goals of this research was to compare the performance of both LEWIS-S configurations (pasted and magnetic) to the pasted strain gauge configured to the commercial DAQ equipment through laboratory testing on a steel cantilever beam. The signal to noise ratio, root-mean-square errors, signal drift, and costs were the primary outcomes for the comparison. Based on the sensor comparison, the LEWIS-S demonstrated results that were comparable to commercial strain sensing equipment. Furthermore, the LEWIS-S presents valuable sensing characteristics such as low costs, wireless capabilities, versatility, and a simple design that is useful for multidisciplinary strain sensing.

During the nonlinear testing the LEWIS-S strain gauge was placed at the root of the beam and a uniaxial accelerometer was placed at the free end. The inertial and geometric nonlinearities were characterized and compared from the responses of both sensors through two different experimental tests. The first test was a sine sweep test where sinusoidal forcing swept across the fundamental resonance of the beam for various increasing forces. The Frequency Response Functions (FRF) and the Continuous Wavelet Transforms (CWT) were

used to compare the responses from the sine sweeps. The second test was a ring-down test where the beam was released from an initial static displacement where the effects of the inertial and geometric nonlinearities were characterized and compared based on the responses from both sensors. The responses from the ring-down tests were compared through time-frequency and amplitude-frequency plots.

A short description of each chapter of this research is provided below:

Chapter 2 of this thesis provides relevant literature that serves as the motivation behind this research. In greater detail, setbacks of using accelerometers for vibration measurements based on placement limitations and added mass and damping to dynamic systems is discussed. Furthermore, using strain gauges as alternatives for vibration measurements is introduced where some common limitations are also identified.

Chapter 3 describes the primary hardware and software components of the LEWIS-S and the relevant theory behind its design and development. The static and dynamic validation testing of the sensor is also introduced, and conclusions are drawn from the laboratory testing concerning the performance and cost.

Chapter 4 introduces the application of the LEWIS-S in measuring the inertial and geometric nonlinearities due to large displacements on the cantilever beam based on sine sweep and ring-down testing. Conclusions are drawn from the testing and are referenced to the analytical solutions from nonlinear theory.

Chapter 5 draws conclusions from the development and performance of the LEWIS-S sensor based on the validation testing. Conclusions from the nonlinear dynamic testing are also made for the comparison of results between the accelerometer and strain gauge. Lastly, the limitations and future work of the sensor are introduced based on the conclusions of the research. Future improvements and modifications regarding the next generation of the LEWIS-S sensor design are also addressed.

Chapter 2 Literature Review

2.1 Introduction

This chapter introduces a brief background on information that serves as the motivation for this work, where common vibration measurement sensors are addressed. The first part discusses accelerometers in the context of common uses and limitations in current research. The second part discusses the use of strain gauges in linear and nonlinear dynamics and highlights a few benefits and limitations in research.

2.2 Common Limitations of Using Accelerometers in Dynamics

Traditionally, accelerometers are widely used for measuring dynamic responses in experimental modal analysis (EMA) testing. These sensors are arguably the most common for both linear and nonlinear modal testing where natural frequencies, mode shapes, and displacements can be identified [16]. As with all sensing methods, there are limitations that render the use of standard accelerometers with cable attachments problematic or impractical in certain applications of EMA testing. It is well documented that the use of accelerometers can occasionally interfere with the dynamics of a system based on the added lumped mass of the sensor body and stiffness and damping from the cables, especially when dealing with lightweight systems [17,18]. There are limitations to the test setup such as when testing in wind tunnels on aircraft wings [19] or systems where accelerometers cannot adhere to surfaces that experience strong centrifugal forces in testing [20].

Additionally, there are hardware size and accessibility limitations for cases when it is difficult to place accelerometers on a system in a particular location such as measuring small components or measuring the dynamic response on the tip of a wind turbine blade, as detailed in [16, 21]. Finally, perhaps a rather trivial limitation, is that accelerometers can only provide acceleration response at a particular location on the structure. This has many advantages, but there may be other quantities of interest from a test that cannot be directly provided using this method. For example, in Figure 3, strain gauges were used to obtain the dynamic response of a helicopter blade and quantify damage.

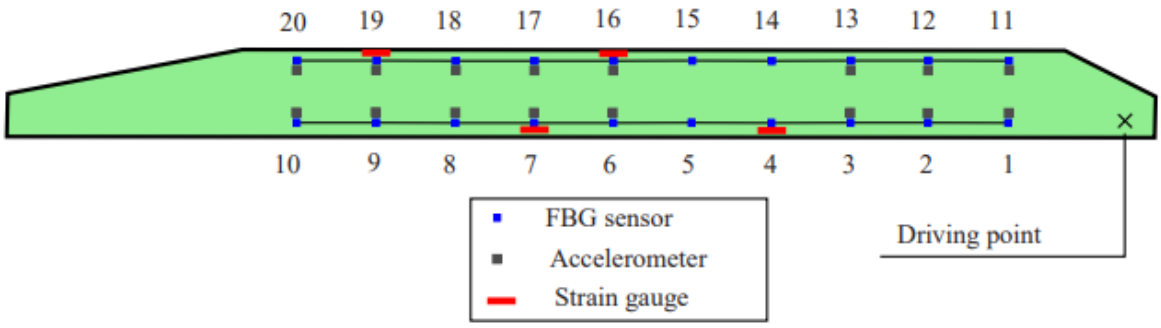

Figure 3 Using strain gauges, accelerometer, and FBG sensors to measure the dynamic response of a helicopter blade [16]

2.3 Strain Gauges in Dynamics

In light of addressing some of the limitations of accelerometers in EMA, strain gauges have commonly been used as alternatives to obtain the dynamic response of a system in order to measure the strain at a particular location along with the spectral content of responses during testing [19]. The use of strain gauges in EMA introduces the ability to monitor strain for

damage detection, fatigue, and durability analyses during linear and nonlinear testing [22, 23-25]. Moreover, as seen in Figure 4, the use of strain gauges in EMA for nonlinear dynamics can be extended to nonlinear modal analyses. As described in [26, 27], strain gauges were used to measure the nonlinear response of a cantilever beam and plate elements.

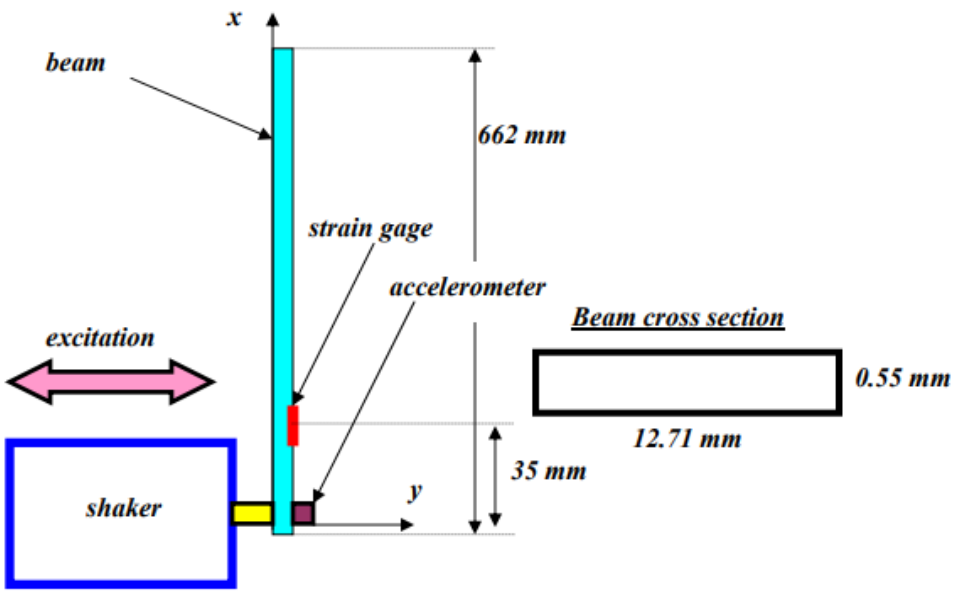

Figure 4 Using a strain gauge to measure the dynamic response of a cantilever beam [27]

The use of strain gauges in nonlinear analyses are additionally commonly used in measuring material nonlinearities where yielding and permanent deformation can be determined to produce nonlinear stress-strain curves [28]. Approximating strains in a nonlinear structure using accelerometers requires the use of a calibrated model, which may be beyond the scope of a test campaign. Therefore, direct measures of strain for nonlinear structures provides a practical and efficient means to obtain the necessary quantities of interest and understand the amplitude dependence of strain with respect to input level.

There are a few common solutions that address some of the limitations of measuring strain that have been used in current research such as portable and wireless sensors. These types of sensors eliminate the need for large and complex DAQ systems by utilizing compact and versatile designs to allow for simplified sensing in the laboratory and field [29,30]. Additionally, as seen in Figure 5, friction-based magnetic strain gauges with wireless capability, have been used in research to enhance strain measurements by significantly decreasing sensor installation times [31].

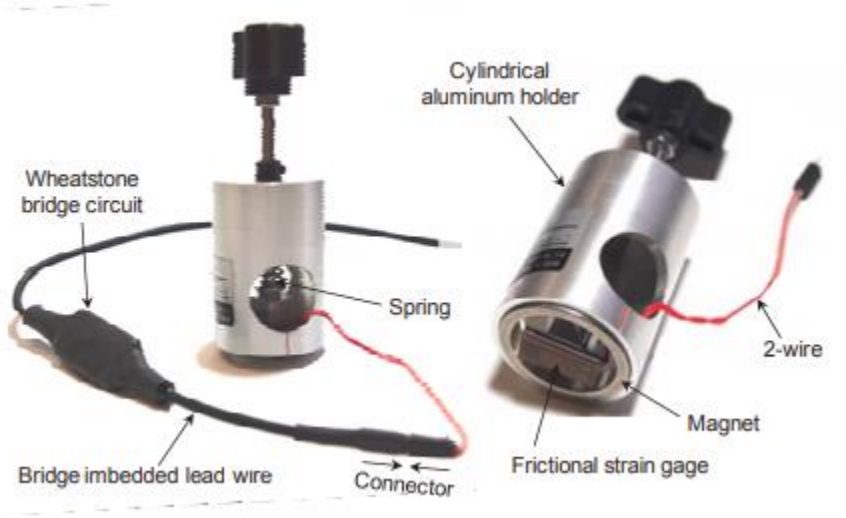

Figure 5 Friction-based magnetic strain gauge [31]

These types of strain sensors add significant measurement capabilities which promote the use of sensor networks and can also introduce new sensing capabilities that otherwise would not have been possible with larger non-portable commercial equipment [32-34]. The networks and smaller size of these sensors can lead to enhanced data collection capabilities by increasing the number of sensors that can be used for testing [35]. However, even these sensors

can still be limiting due to complexity and high costs, especially when custom software is needed for sensor operation.

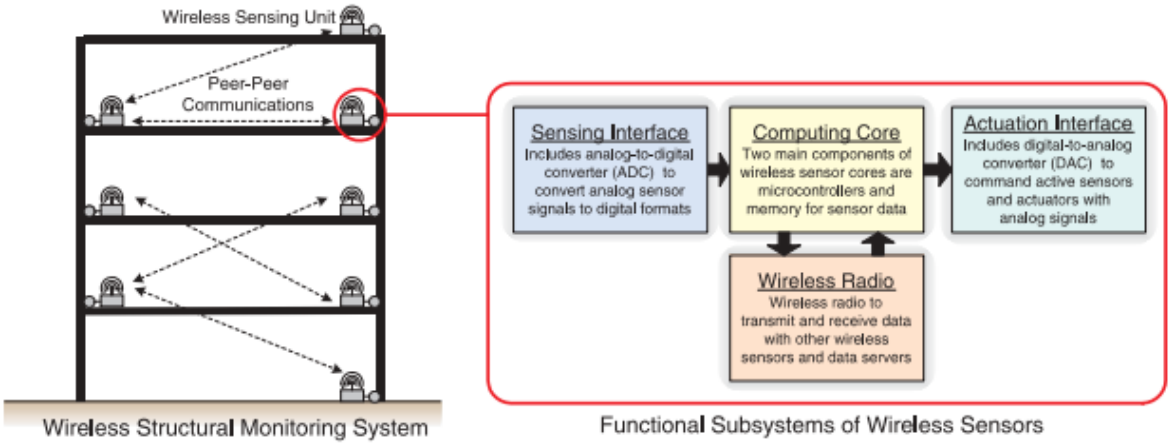

Figure 6 Schematic of wireless sensor structural health monitoring system [34]

2.4 Conclusions

Various research has demonstrated that accelerometers are useful for measuring responses in linear and nonlinear dynamics, however, there are certain limitations in dynamic sensing that strain gauges can address. Strain gauges can resolve some of the limitations such as sensor placement restrictions and the added mass effects of a sensor to a system. Furthermore, current research has shown that low-cost, wireless, and sensor networks can be established to add greater capabilities to strain sensing. However, in consideration of low-cost and wireless sensors, there are still limitations that render these options problematic. It is therefore important to develop a solution that addresses the limitations of complex acquisition and high costs for low-cost and wireless strain sensors.

Chapter 3 LEWIS-S Sensor

3.1 Introduction

This chapter describes the development and testing of the LEWIS-S. The first part of this chapter briefly discusses the hardware and software components on the LEWIS-S sensor and the theoretical foundation that is used for its operation. The second part discusses the different configurations of the LEWIS-S sensor used for the validation testing against the commercial DAQ. Next, the experimental setup is detailed where the static and dynamic validation testing is conducted. The last part of this chapter compares and summarizes the results from the validation testing and comments on the findings.

3.2 LEWIS-S Software

The LEWIS-S uses free Arduino software, also known as Integrated Development Environment (IDE), to write and compile code to the microcontroller. The code for the LEWIS-S primarily needs to instruct the amplifier and microSD card to process and store information from the strain gauge. The IDE interface allows users to interact with the system to store and plot data in real time, and to indicate starting and stopping times for data collection. All necessary operations were modularized for portability and ease of customization.

3.3 LEWIS-S Hardware

Strain gauge sensors are resistive sensors, which vary their resistance value in proportion to their deformation [36]. However, this variation is extremely small so different factors must be considered in the physical circuit design where the signal conditioning is going to be carried

out. Therefore, a few critical hardware components were used to handle the signal conditioning on the sensor. Namely, a Wheatstone bridge (using precision resistors and potentiometers), and an amplifier embedded with a 24bit analog-to-digital converter (ADC).

The LEWIS-S is comprised of multiple components assembled on an Arduino Uno Rev 3 development board. The sensor utilizes a Wheatstone bridge, ADC, and amplifier to capture the change in resistance from any type of resistive strain gauge. Additionally, two Xbee radio transceivers are used for wireless data initialization capabilities, and a secure digital (SD) shield is used for data transmission storage to a microSD card. The wireless sensor is powered by a small 7.4 V double cell rechargeable battery; however, the sensor can also be operated through a USB connection or an AC-to-DC power adapter when necessary. Figure 7 depicts the signal conditioning circuit for the strain gauge mounted on the protoboard of the shield, which is responsible for the connection to the microcontroller, the microSD card, and the wireless communication module.

The list of main components the LEWIS-S is comprised of is as follows: Arduino Uno3 development board, Hx711 amplifier, ICSTATION wireless SD shield, two Xbee serial transceivers, a 7.4-volt rechargeable battery, 16GB SD card, and a Wheatstone bridge. It is important to note that each component listed here was individually purchased and manually assembled to create the LEWIS-S sensor. Generally, most components were directly plugged into input and output ports on the Arduino and ICSTATION boards when allowable but various soldered connections were also required to complete the assembly of the sensor.

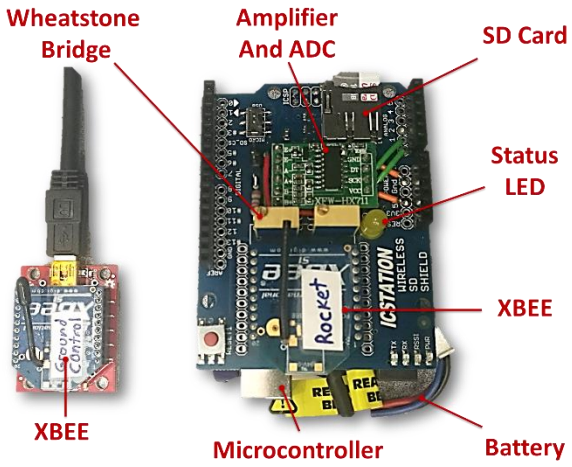

Figure 7 General hardware components of the LEWIS-S sensor

Arduino UNO Rev 3 Development Board

The Arduino UNO Rev 3 is the primary board used for the LEWIS-S which contains an 8-bit Atmega328P microcontroller. The microcontroller has a 16 MHz clock speed, 32 KB flash memory, 2 KB of static random-access memory (SRAM), 1 KB of electrically erasable programmable read-only memory (EEPROM), 14 digital pins, 6 analog pins, and a 5 V peak operating voltage [37]. The primary code was written in Arduino IDE software and is uploaded to the board through a USB connection. The entire board only weighs about 25 grams and is around 2.75 inches by 2 inches.

Hx711 Amplifier

The Hx711 is the amplifier for the output resistance signal from the strain gauges on the LEWIS-S. The amplifier is a 24-bit analog-to-digital converter (ADC) with 16 pins for

multiple input and output configurations. It has selectable gain ranges of 32, 64, and 128 with a sample rate of either 10 samples per second or 85 samples per second and a simultaneous 50 and 60 Hz supply rejection [38]. Since this sensor is an ADC, it requires conversions through shunt calibrations to obtain the micro-strain values from post processing stages. It is important to note that this is the component that limits the LEWIS-S to a low sampling rate.

ICSTATION Shield

The ICSTATION is a digital logic IC wireless SD shield that allows the LEWIS-S to write data to a microSD card through wireless communications through two Xbee transceivers. The shield connects directly into the Arduino Uno board through male and female pins eliminating the need for wiring and soldering. Additionally, the shield has a designated housing directly on the module for the Xbee transceiver and microSD card which allows for direct communication to the microcontroller.

Xbee Transceiver

The Xbee serial transceivers are used on the LEWIS-S sensor to initiate and record data transmission. There are two transceivers used for the sensor, one that connects to a computer and one that connects to the ICSTATION board. Both transceivers have a 2.4 GHz frequency band, 300 ft communication range, 250 kbps data rate, and 128-bit encryption [39]. The primary transceiver configuration platform for the Xbee's requires its own software program, XCTU, in order to connect the transceivers where unique channels can be configured. This

mitigates interference from other sources of signals and to establishes a permanent pairing through unique identification signatures.

USB Converter

A USB to serial base unit is used to connect the base Xbee transceiver to a computer or laptop in order for the transceiver to properly communicate with the transceiver mounted on the SD shield. This produces a USB-to-serial converter for the transceiver which has a voltage regulator, reset button, and LEDs for debugging during configuration [40].

3.4 Fundamental Processes of Sensing

There are three fundamental processes that the LEWIS-S sensor relies on to read and process data. Namely, the mechanics of the Wheatstone bridge, amplification and ADC processes, and the shunt calibration for post processing. The next three sections will describe the backgrounds of these essential hardware processes for the sensor.

3.4.1 Wheatstone Bridge Description

The cornerstone of the LEWIS-S sensor is the Wheatstone bridge circuit which utilizes a set of ratios between resistors in balanced (unloaded) and unbalanced (loaded) states to measure a change in electrical resistance and produce an output voltage [41]. Due to the simple design of the Wheatstone bridge, it is a convenient and simple way to obtain a measurement based on a change in resistance. Figure 8 depicts a general Wheatstone bridge configuration.

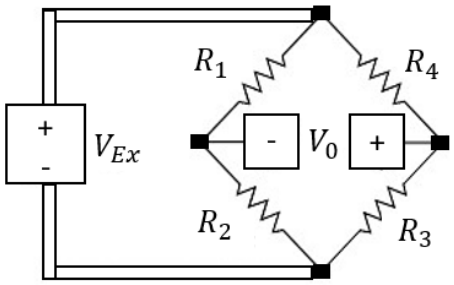

Figure 8 Wheatstone bridge circuit

The quarter bridge circuit utilizes the capability of measuring the output voltage due to the ratio of resistance through the use of four different resistors. As seen in Figure 8, the ratios described in Equation (1) will be satisfied when the output voltage across the resistors equals zero and $R_1 = R_2$, where V_0 is the output voltage and R_S (R_4) is the unloaded resistance of the strain gauge.

$$\frac{R_3}{R_1} = \frac{R_S}{R_2} \tag{1}$$

$$V_0 = \left[\frac{R_3}{R_3 + R_4} - \frac{R_2}{R_1 + R_2}\right] V_{EX} \tag{2}$$

However, when the gauge is loaded there will be a change in resistance and the output voltage will change according to the relationship specified in Equation (2). The output voltage then passes through an amplifier and is recorded as an ADC value where a calibration factor is applied in the post processing in order to obtain the corresponding micro-strain values.

3.4.2 Amplification and Analog to Digital Conversion

It is necessary to use a device to amplify the analog signal and convert it into digital data that can be processed by the microcontroller. In this regard, the integrated circuit HX711 was selected, which meets all the requirements to process the strain gauge sensor signal. This chip, however, does not have a standard communication such as UART or I2C; the data on this chip is obtained by pulsing one of its lines, like the work of a clock. On the other line the digital value (High or Low) for that specific pulse is read. In total, 25 pulses must be executed for the chip to operate using the input channel-A and an amplification with a gain of 128. It is also relevant to mention that the first data bit that comes out is the one corresponding to the Most Significant Bit (MSB) and the last is the Least Significant Bit (LSB), because the data comes out serially and in that order. The algorithm must perform a bit shift to correctly order the 24 bits of data that correspond to a single reading of the system.

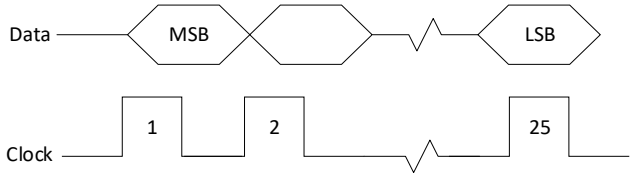

Figure 9 Timing and control diagram for channel-A

After the 24 bits of data is read, a sign conversion is performed, because the whole word is delivered by the HX711 in two's complement format, therefore, after the conversion the data is obtained as shown in Table 1.

Table 1 LEWIS-S ADC conversion factors

	Two's Complement	Converted
Minimum	-8,388,608	0
Zero	0	8,388,608
Maximum	8,388,607	16,777,215

Once the data is read and the corresponding conversion is carried out, it is stored in the microSD card then sent wirelessly through the Xbee module. This is done in order to reduce the computational load in the microcontroller and to keep the sampling frequency to the chip's maximum capacity. The converted values shown in Table 1 is the ADC resolution on the amplifier. Based on the initial equilibrium position of the Wheatstone bridge, the signal can saturate outside of the converted range. Therefore, it is important to keep the signal output near the converted zero value prior to initializing recording. After downloading the data to a computer, the recorded data is converted to micro-strain values.

3.4.3 Shunt Calibration for Post-Processing

Shunt calibrations are an effective way to quickly and accurately calibrate strain gauges that contain Wheatstone bridges [42]. The purpose of the shunt calibration is simply to obtain a calibration factor that describes the relationship between the strain gauge and shunt resistor to the corresponding micro-strain value. In other words, the calibration factor will ultimately convert the ADC values to micro-strain values. The process is done by simply shunting the strain gauge resistor contained in the Wheatstone bridge with another resistor where Equation

(3) is used to determine the strain value associated with the shunting process. Figure 10 summarizes the procedures performed to convert the digital values to micro-strain values through means of the shunt calibration.

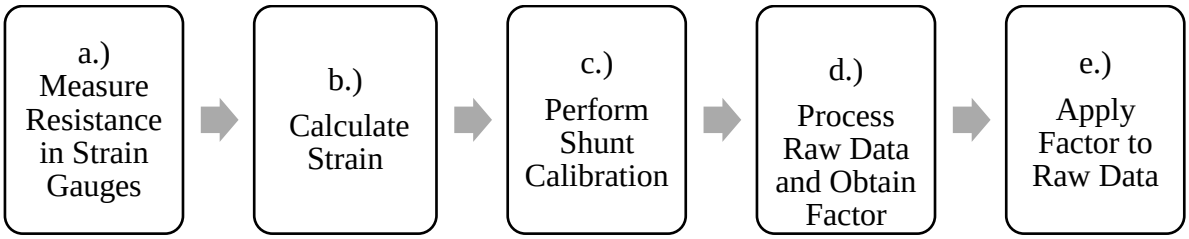

Figure 10 Data post-processing flow diagram

a. Measure Resistance in all Strain Gauges:

The goal of this step was to measure the resistance values of the unloaded SG's using a multimeter. Generally, the SG's retained different resistance values than their nominal resistance values due to the circuitry and added resistance caused by the wired connections.

b. Calculate Strain:

The unloaded resistance values from the multimeter readings for the strain gauge, R_G, the shunt resistor value R_C, and the gauge factors, F_G for each SG were then used to calculate the micro-strain from the shunt calibration.

$$\varepsilon_s = \frac{-R_G}{F_G(R_G + R_C)} \tag{3}$$

c. Perform Shunt Calibration:

The shunt calibration consisted of shunting the unloaded SG with a known resistor value in order to obtain a theoretical value based on the shunt measurement. First, the LEWIS-S sensor was started and kept unloaded (no shunt-resistor connected) for about 30 seconds. Then, a connection was made to the shunt resistor and recorded for 30 seconds. Lastly, the connection was disconnected, and the recording was stopped after another 30 seconds.

d. Process Raw Data and Obtain Shunt Calibration Factor:

The raw calibration data was smoothed using a smooth data command in MATLAB with a moving average. The data was split into three sections that was averaged individually. The first and third sections were the unloaded condition, and the second section was the loaded condition where the shunt resistor was connected to the circuit. The difference between the loaded and unloaded sections was an ADC value that corresponded to the shunt load. The calibration factor was calculated by dividing the strain calculated in Equation (3) by the final ADC value.

e. Apply Factor to Raw Data:

The calibration factor was then applied to the raw data in order to convert the ADC values from the HX711 amplifier to the final strain values. Lastly, the final strain plots were detrended in order to establish a common zero point.

3.5 Commercial and LEWIS-S Configurations

Two LEWIS-S sensors were developed for the validation testing in this research where one sensor utilized a traditional pasted uniaxial linear resistive strain gauge attachment whereas the second utilized a magnetic friction-based uniaxial linear resistive strain gauge. The only difference between the two configurations was the Wheatstone bridge circuit. The LEWIS-S pasted configuration (LEWIS-S1) required the design and assembly of an external Wheatstone bridge circuit whereas the LEWIS-S magnetic configuration (LEWIS-S2) had an internal Wheatstone bridge circuit embedded in its casing. The remaining hardware components and software were the same between the two configurations during the testing. The two LEWIS-S configurations were compared to a traditional commercial DAQ system shown in the following sections. Table 2 breaks down the cost, size, and configuration time between the LEWIS-S and commercial equipment. The LEWIS-S demonstrates a significant advantage over the commercial equipment through cost and size characteristics.

Table 2 Cost and size comparison of LEWIS and commercial equipment

Description	**LEWIS-S (Without SG Attachments)**	**Commercial**
Cost of Hardware	< $225 USD	$5000-$10,000+ USD
Cost of Software	Free	Free - $5000+ USD
Area of Footprint (plan-view footprint)	$< 0.25\ ft^2$	$> 1\ ft^2$

3.5.1 Configuration 1: Commercial DAQ with Pasted Strain Gauge Attachment

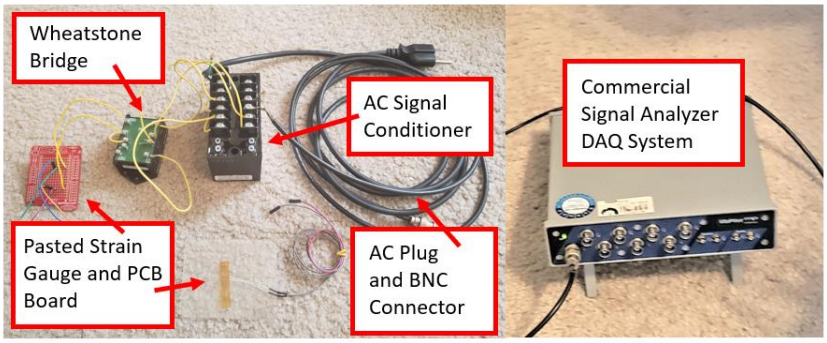

Figure 11 Commercial DAQ configuration

The benchmark commercial equipment that the two LEWIS-S configurations were compared to during experimental testing is shown in Figure 11. The commercial DAQ system utilizes a comprehensive software program to control input forces from the load and the output response from the sensors. For the purpose of the experimental testing in this research, the commercial DAQ used a sampling rate of 1024 Hz for the strain measurements but it does have adjustable sampling rates that can be increased or decreased. The strain gauge attachment configured to the commercial DAQ that was used during validation testing was the same pasted strain gauge attachment on the LEWIS-S1 configuration. The commercial DAQ configuration consists of an external Wheatstone bridge, an AC signal conditioner, and a signal analyzer to measure and process data. The commercial equipment required approximately 12 wires to operate, two of which were an AC power source, and a plan-view-footprint of over 1 ft^2.

3.5.2 Configuration 2: LEWIS-S with Pasted Strain Gauge Attachment (LEWIS-S1)

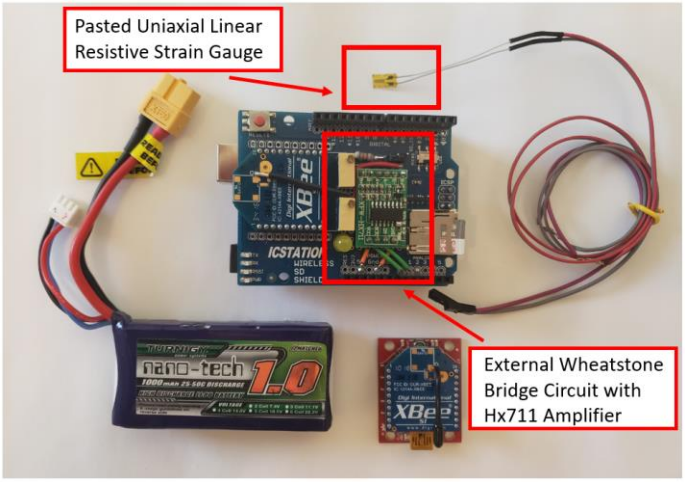

Figure 12 First LEWIS-S configuration with HBM K-CLY41 linear resistive pasted strain gauge

The LEWIS-S1 configuration required an external Wheatstone bridge as seen in Figure 12 due to the type of strain gauge used. The external circuit retains two potentiometers, which can be manually adjusted to balance the bridge, the strain gauge, a 120-ohm resistor, the Hx711 amplifier, and a status indicator LED.

The first strain gauge that was configured on the LEWIS-S was the Hottinger Baldwin Measurements (HBM) K-CLY41 foil strain gauge. This strain gauge is a linear resistive gauge made from a polyimide carrier, constantan measuring grid and 50mm fluoropolymer-insulated wires shield [43]. The gauge has a nominal resistance of 120 ohms and has two nickel-plated copper leads which connect to an external Wheatstone bridge circuit on the wireless SD shield. This specific linear gauge will only measure strain along its longitudinal axis and is solely designed to measure strain on ferritic steel materials where it is generally recommended from

the manufacturer that the gauge is properly calibrated, acclimated to its environment, and correctly pasted to the material before testing.

3.5.3 Configuration 3: LEWIS-S with Magnetic Strain Gauge Attachment (LEWIS-S2)

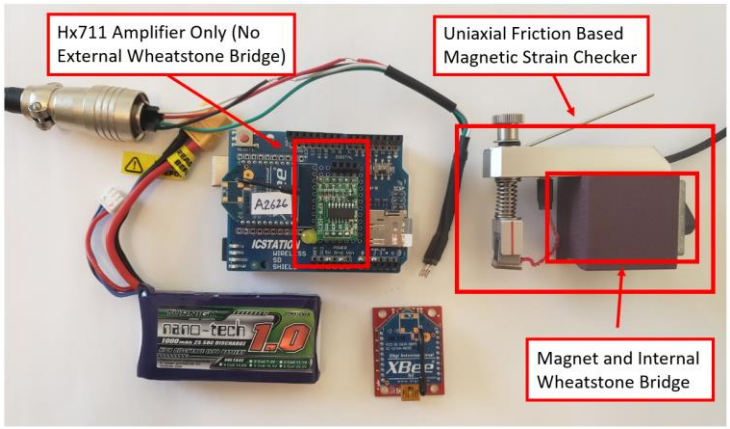

Figure 13 Second LEWIS-S configuration with FGMH-2A single axis frictional magnetic strain gauge

The LEWIS-S2 configuration uses the FGMH-2A frictional strain checker from Tokyo Measuring Instruments Laboratory which measures strain through frictional contact induced by a magnetic force which eliminates the need for pasting [44]. The magnetic strain gauge attachment eliminates the need for an external Wheatstone bridge circuit on the Arduino board as this gauge includes the bridge circuit in the sensor's encasement. This simplifies the LEWIS-S design to just the Hx711 amplifier and the other general sensor hardware however, it does slightly increase the overall cost of this configuration. The friction-based magnetic gauge demonstrates the versatility of the LEWIS-S and introduces a convenient addition to strain sensing by eliminating the need of timely traditional strain gauge pasting processes.

3.6 Static and Dynamic Experimental Validation Tests

Researchers at the Smart Management of Infrastructure Laboratory (SMILab) at the University of New Mexico (UNM) conducted laboratory tests in a controlled and repeatable environment to validate the function and accuracy of the LEWIS-S in static and dynamic testing conditions. Both tests were conducted to compare and validate the LEWIS-S1 and the LEWIS-S2 to the traditional commercial DAQ system, which acted as the benchmark for the tests. The first test compared the three sensors in static loading conditions on a simple cantilever beam with three different point load masses suspended at the free end of the beam. The second test compared the three sensors in dynamic loading conditions on the same beam with a small modal shaker attached in the same location on the free end of the beam. The purpose of these tests was to observe and quantify the performance of the two LEWIS-S configurations in both test conditions and compare them to the commercial DAQ system. As a result, the curves of each test were analyzed together to observe the characteristics of the overall fit.

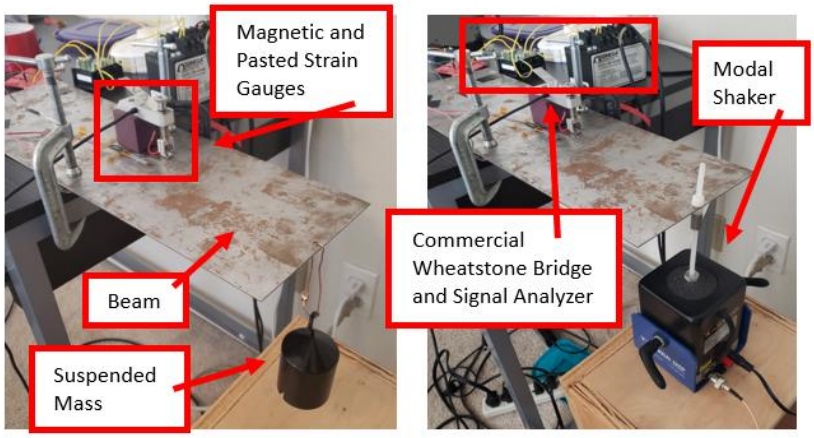

(a) (b)

Figure 14 Static load test with 1 kg mass (a) and dynamic load test with modal shaker (b)

3.7 Static Testing

In the static test a theoretical strain value was used to assess the quality of the commercial sensor measurements during the comparison. The cantilever beam was set with two C-clamps on the edge of a rigid table where a series of three short tests were conducted, each with different masses. Each mass was suspended from a flexible wire tied through a hole at the edge of the beam and remained perpendicular to the ground throughout the beams deformed state. Figure 15 depicts the layout of the sensors where the LEWIS-S2 and commercial strain gauge configurations were configured on the top of the beam near the clamped end, whereas the LEWIS-S1 was configured directly below them on the underside of the beam.

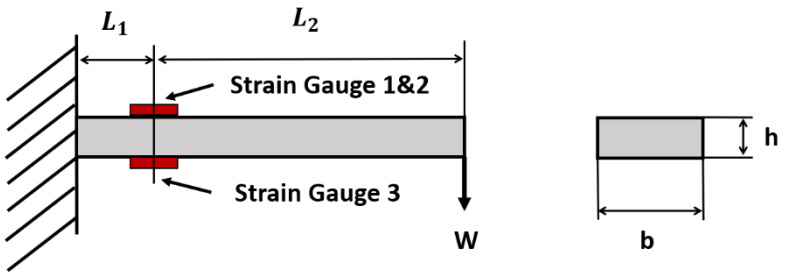

Figure 15 Cantilevered beam dimension and loading test description

The theoretical strain was calculated by utilizing the relationship in Equation (4) where strain values will retain the greatest amplitude at a location closest to the clamped end of the beam, where the largest moment is generated. This concept was considered for selecting the location of the strain to be calculated to assure there was a large enough magnitude for the sensors to measure and also so the response could be qualitatively assessed. Table 3 describes the physical properties of the cantilever beam used during the experimental testing.

$$\varepsilon = \frac{Mc}{EI} \tag{4}$$

Table 3 Mechanical Properties of Cantilever Beam

EI $(K\ in^2)$	$\boldsymbol{L_1}$ *(in)*	$\boldsymbol{L_2}$ *(in)*	**b** *(in)*	**h** *(in)*
3.1	1	7.5	6.01	0.059

3.7.1 Static Test Results

The results from the three static tests demonstrated a great agreement between the three sensors. As seen in Figure 16, there are three segments that comprise each curve with approximately equal timespans. For each load case the first (pre-loading) and last (post-loading) segments represented the unloaded beam condition whereas the mid-section represented the loaded condition. This was an important characteristic for this testing because it demonstrated how well each sensor could capture data and recover, in terms of drift, from the static load.

Generally, since the LEWIS-S1 configuration required an external Wheatstone bridge where two potentiometers were used to zero the sensor at rest, the bridge can become slightly unbalanced during testing which causes the signal to drift after cyclic loading. Therefore, this was carefully observed during the testing. A poor recovery condition can be seen in Figure 16 (a) and (b) in the 60-90 seconds region where the LEWIS-S1 sensor failed to return to a its unloaded position which is attributed to drift.

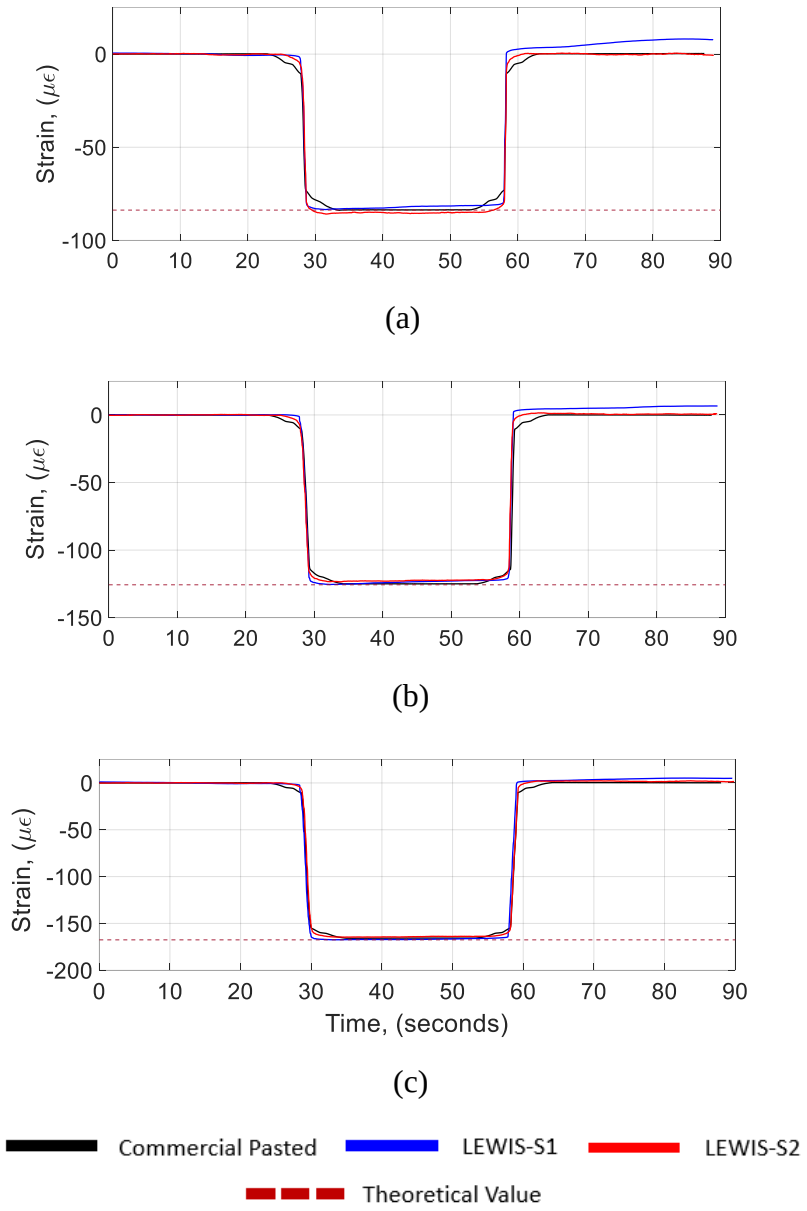

Figure 16 Static point load test results for all SG's, (a) 0.5 kg, (b) 0.75 kg, and (c) 1 kg

It is important to note that the strain response from the commercial DAQ system inherently varied from the theoretical strain for each test by 1% or under, as seen in Table 4. This can be attributed to various factors such as a difference in the beam's modulus of elasticity, small errors in the beam's dimensions, and small errors in the data post-processing.

Based on the results shown in Table 4 the commercial configuration produced the most accurate result with respect to the theoretical value with an average error of under 1%. The average errors of the strain measurements using the LEWIS-S1 and LEWIS-S2 were 1.75% and 4.66%, respectively. The LEWIS-S2 retained the largest error of all three sensors at a peak of 6.11%, whereas the LEWIS-S1 and commercial configurations retained peak errors of 2.45% and 1.11%. The larger errors from the two LEWIS configurations can be attributed to slight signal drift and inherent noise produced by the microcontroller.

Table 4 Summary of results and errors for all sensors in static loading

Sensor and Load	**Average** ($\mu\varepsilon$)	**Error** (%)
Commercial 0.5 kg	-83.48	0.33%
Commercial 0.75 kg	-124.92	0.57%
Commercial 1 kg	-165.65	1.11%
Average Error		**0.67%**
LEWIS-S1 0.5 kg	-81.71	2.45%
LEWIS-S1 0.75 kg	-123.18	1.95%
LEWIS-S1 1 kg	-166.08	0.85%
Average Error		**1.75%**
LEWIS-S2 0.5 kg	-81.94	2.17%
LEWIS-S2 0.75 kg	-117.96	6.11%
LEWIS-S2 1 kg	-157.94	5.71%
Average Error		**4.66%**

3.8 Dynamic Testing

Four dynamic tests were conducted on the cantilever beam with both LEWIS-S configurations and the commercial DAQ setup. A simple forced sine wave was induced on the beam for the first three tests. The main goal of this test was to observe the quality of data obtained by the two LEWIS-S configurations in a simple dynamic state at low frequencies through comparing signal to noise ratios (SNR), signal drift, root mean square errors, and the effects of sampling rates. Each dynamic test was conducted at low frequencies in order to obtain the largest possible displacement from the modal shaker.

It is important to note that all the results from the tests obtained in this section had to be manually started and stopped at approximately the same time, so there were minor inherent discrepancies between the time vectors along the x-axis. This is particularly evident in the beginning of the sine test at 1 Hz, Figure 17 (a) and the end of the sine tests at 2 Hz and 3 Hz, Figures 17 (b) and (c).

3.8.1 Sinusoidal Signal Test Results

After the shunt calibration of each sensor was performed and the corresponding micro-strain value was obtained, each response was detrended, and overlaid. Figure 17 demonstrates the results of the three sensor configurations, where the LEWIS-S1 and LEWIS-S2 were plotted over the commercial configuration. The forcing amplitude on the modal shaker slightly increased as a result of the change in forcing frequency. It can be seen in Figure 17 (a) and (b) that the response from LEWIS-S1 sensor contained more noise which resulted in inconsistent peak amplitudes. The noise of the three sensors is quantified in Table 5.

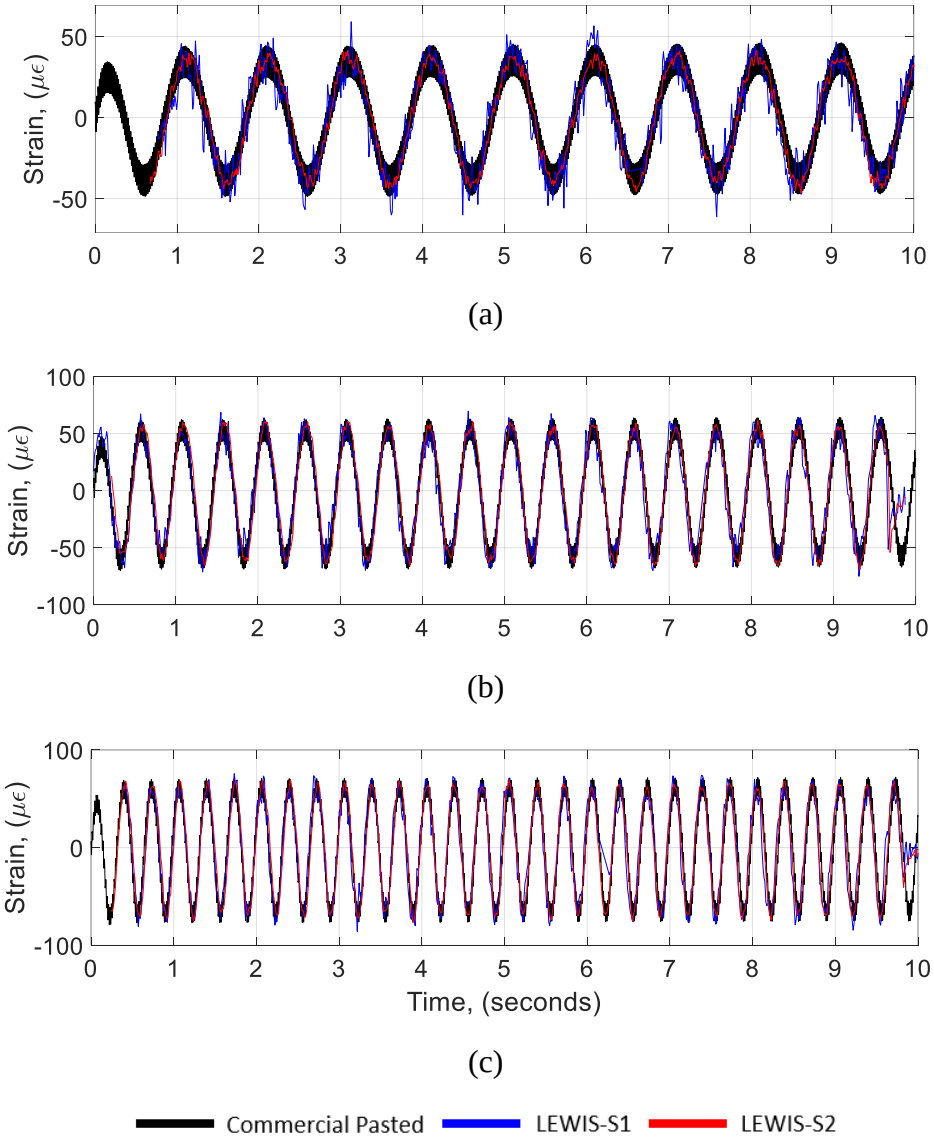

Figure 17 Dynamic test results for all SG's, (a) 1 Hz, (b) 2 Hz, and (c) 3 Hz

The signal to noise ratios (SNR) of each sensor in the sine testing were considered in order to quantify which configuration produced the most accurate response. The SNR was calculated by converting the raw signal into a modified periodogram through the power spectral density. The spectral content was used to identify the first six harmonics where the fundamental harmonic was used as the signal and the remaining data was processed to identify the noise. The SNR of each response was calculated by using Equation (5), where larger values corresponded to less noise.

$$SNR = 10log_{10}\left(\frac{ENBW * PSD_{signal}}{\frac{1}{N}\sum_{i}^{N} PSD_{i\ noise}}\right) \quad (5)$$

The signal shown in the numerator in Equation (5) is the power of the fundamental harmonic, PSD_{signal}, multiplied by the two-sided equivalent noise bandwidth, $ENBW$. The noise, PSD_{noise}, was calculated by determining the median power of the data outside of the harmonics and DC content where the mean of the extrapolated noise density inside the harmonic, DC, and signal regions was included. Table 5 summarizes the SNR's for the three forcing frequencies for each sensor configuration.

Table 5 Signal to noise ration of each sensor in sine tests

Frequency (Hz)	Commercial (dBc)	LEWIS-S1 (dBc)	LEWIS-S2 (dBc)
1 Hz	12.8	9.94	20.24
2 Hz	16.37	14.82	22.52
3 Hz	17.58	11.69	18.12

Based on the SNRs documented in Table 5, the LEWIS-S2 had the largest SNR values for each frequency test, whereas the LEWIS-S1 had the lowest SNR values for each frequency test. However, the commercial sensor had larger SNR values compared to the LEWIS-S1 but had approximately 23% more noise than the LEWIS-S2 SNR values, on average. This suggests the LEWIS-S2 sensor contained the lowest amount of noise in each response. The noise from the LEWIS-S1 is apparent in Figure 17 (a) where various transient spikes can be seen in the response, whereas the LEWIS-S2 and commercial responses closely follow the underlying 1 Hz sine wave.

In light of the 1 Hz sine wave producing the maximum noise in the dynamic test responses (SNR of 9.94 dBc from the LEWIS-S1), the responses in the 1 Hz test were considered for further comparison. More specifically, the response from each sensor was compared to an underlying, true 1 Hz signal where the root mean square error (RMSE) was computed between the sensor response and the underlying sine wave. The results are presented in Table 6. In a more practical context, the RMSE from the 1 Hz test depicts the average difference in micro-strain with respect to the true response.

Table 6 Root mean square error of each sensor in the 1 Hz dynamic test

Commercial (με)	**LEWIS-S1** (με)	**LEWIS-S2** (με)
6.8	9.5	5

3.8.2 Random Signal Test Results

The random signal dynamic experiment was conducted to primarily analyze the response of the three configurations in the frequency domain to compare the frequency content from each sensor. Since the aim of the dynamic tests were not to determine the natural frequencies of the beam, there was no isolated fundamental harmonic in the spectral data. The dynamic experiment for the random signal was conducted at very low frequencies, namely, between 1 Hz and 4 Hz so this bandwidth in the frequency domain was the center of consideration to assess the agreement between the configurations.

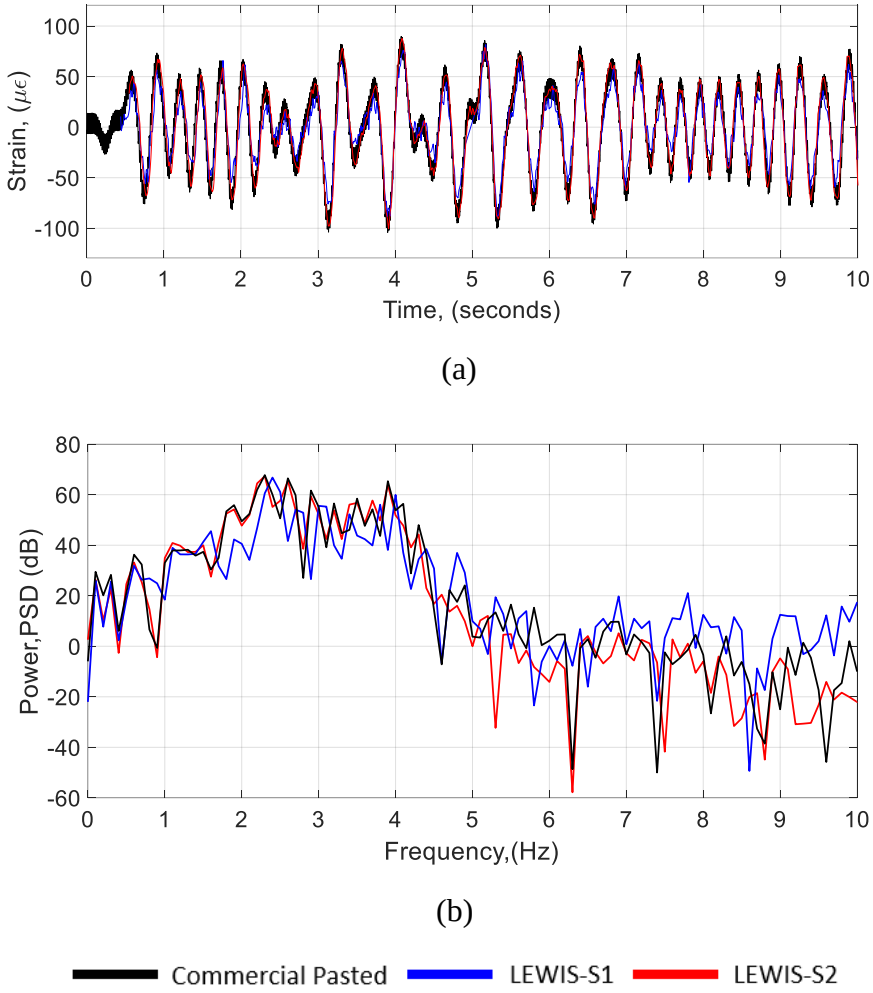

Figure 18 Strain response time-history (a) and frequency content (b) of random signal

It can be observed in Figure 18 (b) that the LEWIS-S1 retained the worst performance in the frequency domain, likely attributed to the low SNR in the time-history signal and the imperfect balance of the Wheatstone bridge. The LEWIS-S2 performed well as great agreement to the commercial configuration can be observed in the 1 Hz to 4 Hz bandwidth. However, there is a small but distinguishable departure between the LEWIS-S2 and commercial sensor frequency responses after 4 Hz and a large departure between the LEWIS-S1 and commercial responses after the same frequency. The most critical aspects of the sensor

comparison for this research have been summarized in Figure 19 where the y-axis represents the normalized values specified by the x-axis labels. Figure 19 compares the cost, footprint, dynamic test error, static test error, and the signal to noise ratio (SNR) for all configurations. Note that the signal drift, which was considered in the analysis, was not compared in Figure 19. Also note that a value of 1 in the SNR comparison corresponds to a better signal (less noise). Lastly, the cost and footprint include the strain gauge (SG) attachments with the general LEWIS-S sensor body and components.

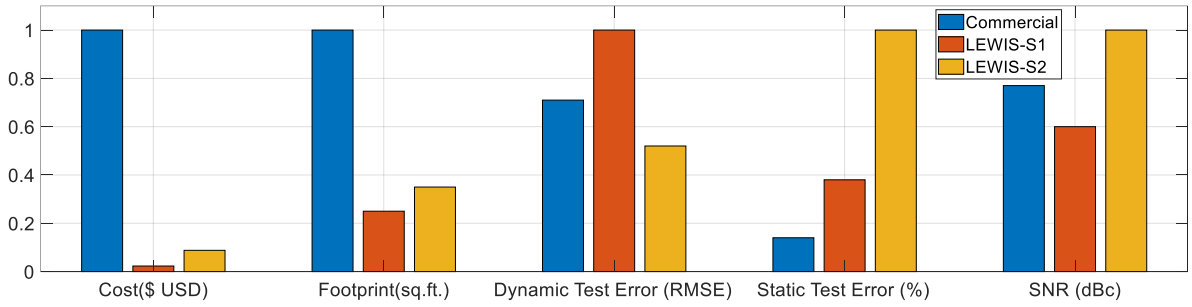

Figure 19 Comparison of advantages and disadvantages of all sensor configurations

3.9 Conclusions

It is important to reinforce that the goal of the LEWIS-S development was not necessarily to create a sensor to perform better than the commercial equipment but rather to create a low-cost and wireless sensing solution that is reliable and accurate to a degree that is comparable to commercial equipment. Based on the results of the static and dynamic test comparisons presented in this chapter, the two LEWIS-S configurations had varying measurement capabilities where their strengths generally traded off between the test errors. However, it was demonstrated that the LEWIS-S sensor retained a significant advantage of cost and portability over the commercial configuration.

Chapter 4 Large Displacements of a Cantilever Beam

4.1 Introduction

This chapter describes the testing of the LEWIS-S on a cantilever beam with large displacements. The first part of this chapter introduces the relevant types of nonlinearity the beam will experience based on large displacements described from an analytical frequency response function. The next part describes the LEWIS-S and accelerometer sensor placement on the beam and the general parameters and setup of the beam and shaker. Lastly, sine sweep, and ring-down testing is introduced where analyses such as the frequency response function (FRF), continuous wavelet transform (CWT), and backbone curves examine the nonlinear behavior in the responses from the accelerometer and LEWIS-S.

4.2 Analytical Solution of Nonlinear Response from Large Displacements

As detailed in [45], the flexural-flexural motion of a nonlinear cantilever beam was found by using the extended Hamilton principle to derive the nonlinear partial-differential equations of motion. The beam is considered to be isotropic, inextensible, and linear elastic that follows Euler-Bernoulli beam theory. The perturbation method was used to obtain the approximate analytical solution for a single-degree-of-freedom system with weak cubic geometric and inertia nonlinearities.

The analytical solution of the frequency-response function is shown in Equation (6) that relates the excitation frequency, $\sigma_{1,2}$ to the response amplitude, a. These were the two unknown variables in the analytical solution. The analytical solution is comprised of two parts, σ_1 and σ_2 where σ_1 represents the right side of the frequency response curve whereas σ_2

represents the left side of the frequency response curve. The analytical solution was plotted in Figure 20 by selecting values through a range of response amplitudes and finding the corresponding excitation frequency for different levels of force.

$$\sigma_{1,2} = \frac{\alpha a^2}{4\omega_n} \pm \sqrt{\frac{f^2}{4{\omega_n}^2 a^2} - (\mu + ca)^2} \tag{6}$$

Where f is the forcing amplitude, ω_n is the *n*th natural frequency of the beam, c is the damping coefficient α is the nonlinearity that is the sum of the geometric and inertia nonlinear terms. The scalar terms corresponding to the properties of the cantilever beam are defined in Equations (7)-(12).

$$\mu = \xi\omega_n \tag{7}$$

$$c = \frac{4\omega_n}{3\pi}\bar{c}\int_0^l {\Phi_n}^2 |\Phi_n|\, ds \tag{8}$$

$$f = a_b \int_0^l \Phi_n \, ds \tag{9}$$

$$\alpha_g = \frac{3EI}{m}\int_0^l {\Phi_n}'(s)^2 {\Phi_n}''(s)^2 \, ds \tag{10}$$

$$\alpha_i = -{\omega_n}^2 \int_0^l \left(\int_0^s {\Phi_n}'(s)^2 \, ds\right)^2 ds \tag{11}$$

$$\alpha = \alpha_i + \alpha_g \tag{12}$$

In these equations, m is the mass per unit length, E is the modulus of elasticity, I is the moment of inertia, ξ is the linear damping factor, a_b is the base acceleration of the beam, l is the length of the beam, $\bar{c}$ is the quadratic damping coefficient, Φ_n is the normalized nth mode shape, and s is the arclength.

Figure 20 depicts an arbitrary example of generating frequency response curves from Equation (6) that demonstrate nonlinear softening and hardening effects from a change in the parameter, α. In Figure 20 a and $\sigma_{1,2}$ were plotted by keeping the forcing amplitude constant while varying the excitation frequency over a resonant mode. This is repeated for several force levels to observe the distortion of the resonant peak for different cases of softening, hardening, and linear behavior. Figure 20 (a) demonstrates a softening effect which occurs when α is negative in Equation (7), where the inertia nonlinear term dominates. Conversely, Figure 20 (c) shows a hardening effect occurring when α is positive, where the geometric nonlinear term dominates. When α is zero the frequency response curves will behave linearly, where no softening or hardening occurs with an increase in force, as depicted in Figure 20 (b).

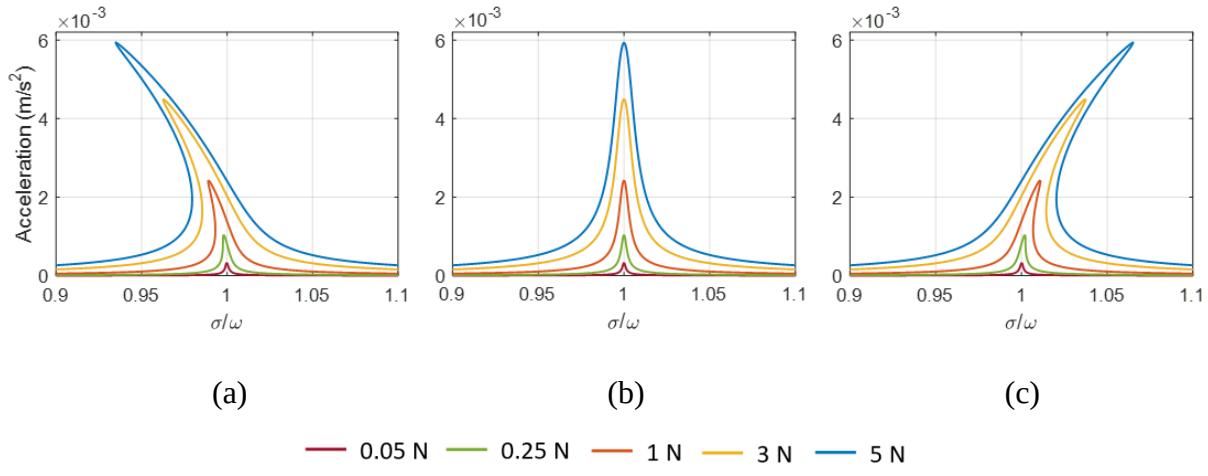

Figure 20 Frequency response curves of increasing force demonstrating the nonlinear softening effect (a), the linear response (b), and the nonlinear hardening effect (c)

As stated in [45] inertia nonlinearities are caused by the kinetic energy in the system which are attributed by centripetal and Coriolis accelerations. Conversely, geometric nonlinearities are caused by the potential energy in the system and are attributed by nonlinear strain and curvature displacements due to large deformations or large-angle motion. As such, it is important to point out that hardening or softening depends on the parameters of the beam such as the length, natural frequencies, stiffness, location of the forcing, etc. Table 7 shows the values used for computing the frequency response curves from Figure 20.

Table 7 Parameters used to compute the analytical frequency response curves

Property	**Value**
ω_n	98π
c	200
α	$-7 * 10^8, 0, 7 * 10^8$
ξ	$6 * 10^{-4}$
f	0.05, 0.25, 1, 3, 5
μ	$\xi * \omega_n$
a	[0:250]

4.3 Cantilever Beam Setup

The LEWIS-S1 configuration was used here where the 120-ohm resistive strain gauge was pasted directly to the root of the cantilever beam as seen in Figure 21. The resistive strain gauge was connected to the LEWIS-S sensor by two wires and the sensor was placed on the rigid test frame so as to not affect the dynamics of the beam.

A cantilever beam was clamped in a vertical configuration where an accelerometer was used to measure the response at the free end and a strain gauge was pasted with an adhesive bond at the base under the shaker. The smart shaker was bolted and clamped to a rigid frame and a load cell was then connected to the smart shaker stinger, which was attached to the beam through a magnet. The smart shaker, load cell, and accelerometer were controlled and recorded through a traditional DAQ system where the force and acceleration retained the same sampling rates of 1024 Hz. Closed loop control was used for the shaker input force and the shaker had a maximum of 7 pounds of forces output. The beam, rigid frame, smart shaker, strain gauge, accelerometer, and load cell layout are depicted in Figure 21.

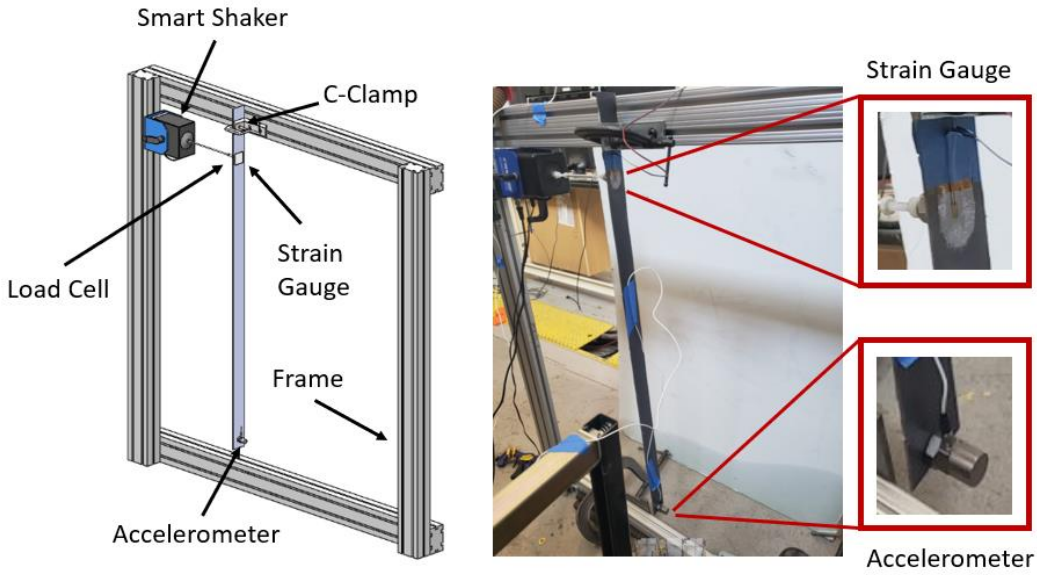

Figure 21 View of cantilever beam experimental setup

Table 8 shows the mechanical properties of the cantilever beam used during the experimental testing. A long and slender beam was selected for this testing to maximize the inertial and geometric nonlinear responses based on low input forces at the root of the beam.

Table 8 Mechanical properties of cantilever beam

Property	**Value**
Flexural Stiffness, EI	1.997 $(K * in^2)$
Width, w	1.75 (in)
Thickness, t	0.077 (in)
Length, L	36.75 (in)
Mass, m	591 (g)
Load Cell Location (from top), LC_L	2.25 (in)
Strain Gauge Location (from top), SG_L	1.75 (in)
Accelerometer Location (from top), A_L	36.5 (in)
Natural Frequency, W_n	1.56 (Hz)

4.3.1 Effects of Accelerometer on a Dynamic Response

Two linear ring-down tests were conducted on the cantilever beam setup, one with the accelerometer at the tip of the beam and a second one without it, in order to compare the effect of the added mass with regard to the fundamental resonance of the beam. In these tests, the LEWIS-S sensor was attached near the beam root for both cases. The beam tip was released from an arbitrary static displacement where the response was recorded by the LEWIS-S sensor

for 45 seconds. The frequency response measured with the accelerometer had a natural frequency of 1.586 Hz whereas the response without the accelerometer had a frequency of 1.782 Hz. the effect of the accelerometer changed the first natural frequency of the beam by approximately 10% as seen in Figure 22 (a).

Furthermore, the envelope of the time histories was also plotted in Figure 22 (b) to demonstrate the effects of damping from the accelerometer wiring. The logarithmic decrement method was used to determine the damping from each response where the accelerometer had approximately 0.35% damping whereas the strain response had 0.24% damping, meaning the accelerometer cables added about 33% more damping. The envelope of each time history response was plotted with a set of nine points corresponding to the same 10 second time intervals in order to quantify how the response amplitudes converged over time. Based on the vertical difference between each set of points the response with the accelerometer converged quicker thus validating the logarithmic decrement calculation.

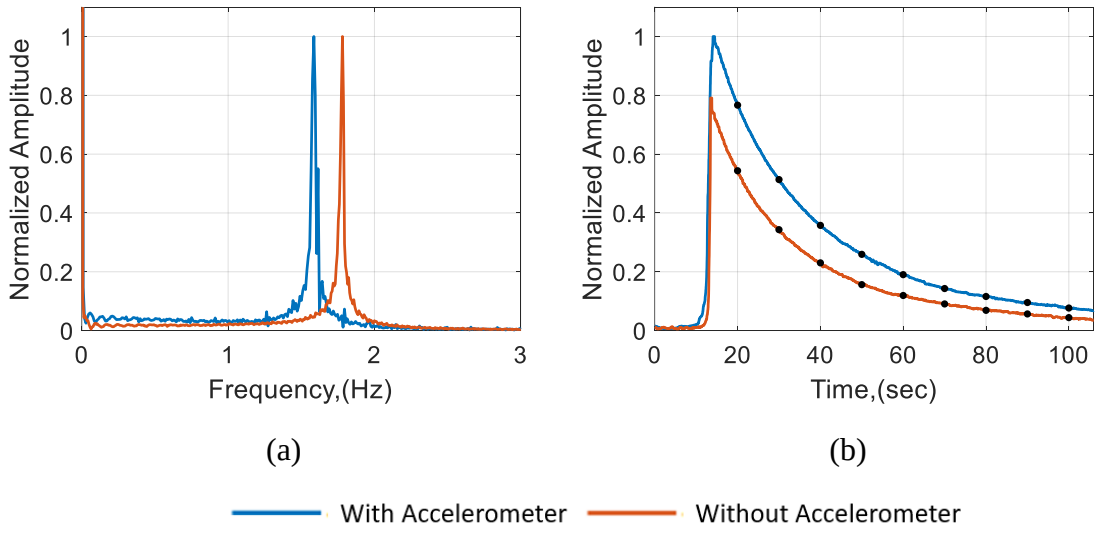

Figure 22 Ring-down strain-frequency response comparison of beam with and without accelerometer (a) and envelope of the time history response of the response with and without the accelerometer (b)

It is important to note here that the response of the accelerometer was used in the experimental testing to validate the results of the LEWIS-S strain gauge. All data beyond this point is used with the both the strain gauge and the accelerometer attached to the beam to measure the vibration responses.

4.4 Sine Sweep Testing

Sine sweep testing was conducted in order to obtain the nonlinear response of the cantilever beam. First, the fundamental mode of the beam was approximated experimentally with a low-level sine sweep test from 1 Hz to 3 Hz. The first linear mode was identified to be 1.56 Hz. Next, a series of seven forward sine sweeps were performed with a starting frequency of 1.45 Hz and ending frequency of 1.65 Hz. The sweep rate was carefully selected to optimize the test conditions for achieving approximate steady state responses and reasonable testing times. Therefore, a rate of 0.02 Hz per minute was used.

Sine sweep tests were conducted where the input force was held constant for the entire test. The input force on the beam was controlled by closed loop feedback control from the DAQ where a load cell was used as the feedback sensor. The plot in Figure 23 shows the measured forces during the sine sweep tests.

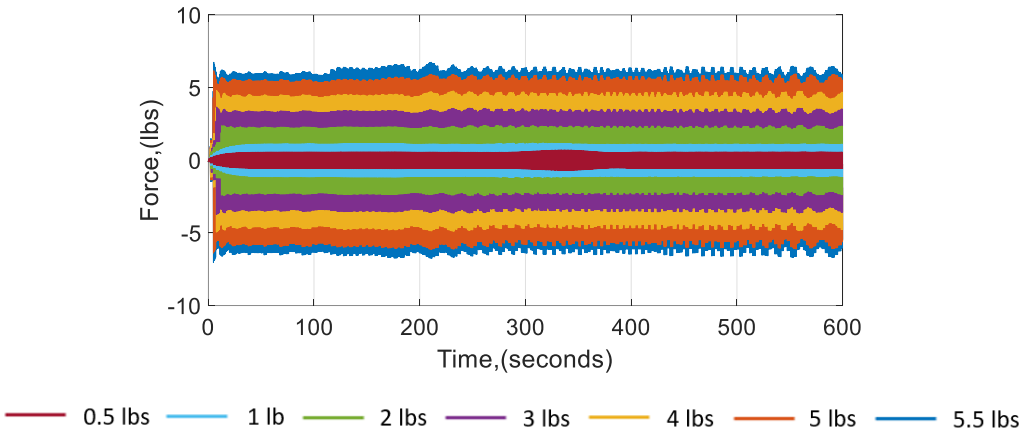

Figure 23 Time-history of force input on cantilever beam

Figure 24 displays the acceleration and strain as a function of the instantaneous sweep frequency. It is noted that the peak amplitude of the strain obtained by the LEWIS-S was approximately 1140 micro-strain and the peak amplitude from the accelerometer was approximately 3 g's. The peak displacement of the tip of the beam was approximated to be 11 inches from the equilibrium position by integrating the acceleration twice to convert acceleration amplitude to displacement amplitude.

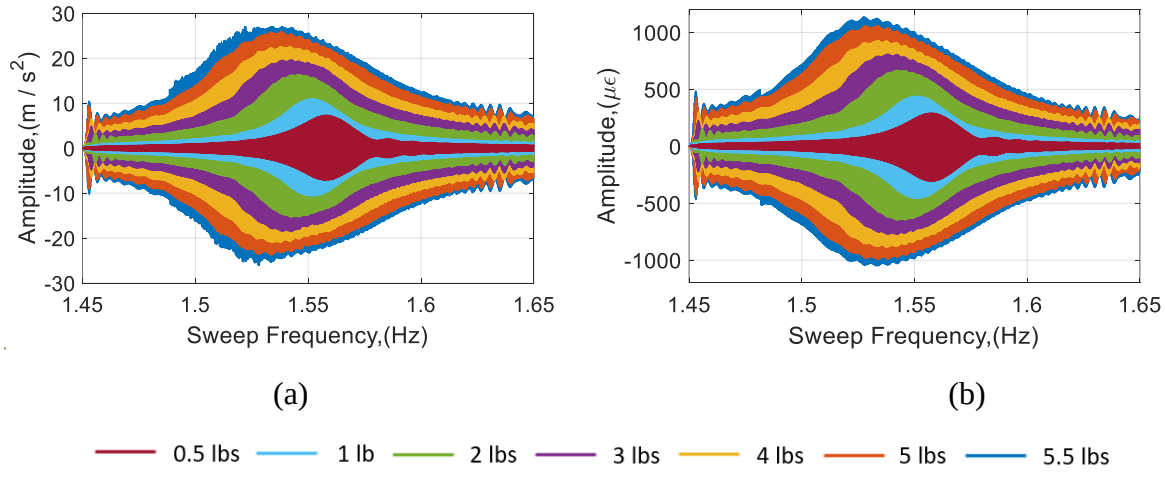

Figure 24 Sine sweep frequency responses from accelerometer (a) and LEWIS-S (b)

The data from both the accelerometer and strain gauge reveal there is a softening behavior in the beam as the force level increases in the sine sweep excitation. This confirms that the nonlinearity in the beam is activated during the selected range of tests. Based on the analysis in Section 2, the nonlinear cantilever beam is dominated by the inertia nonlinearity term due to the observed softening. The sine sweep data is further investigated by normalizing the measured response to the input force and plotting the Continuous Wavelet Transforms (CWTs).

The response from the LEWIS-S was resampled from 86 Hz to the same sampling rate as the forcing signal at 1024 Hz, by using data interpolation. The results were filtered using a moving average filter where the FRF from the accelerometer and LEWIS-S responses were then plotted, which can be seen in Figure 25. The FRF plots show the amplitude-dependent characteristic of the nonlinear response at different forcing levels around the fundamental resonance of the beam [46].

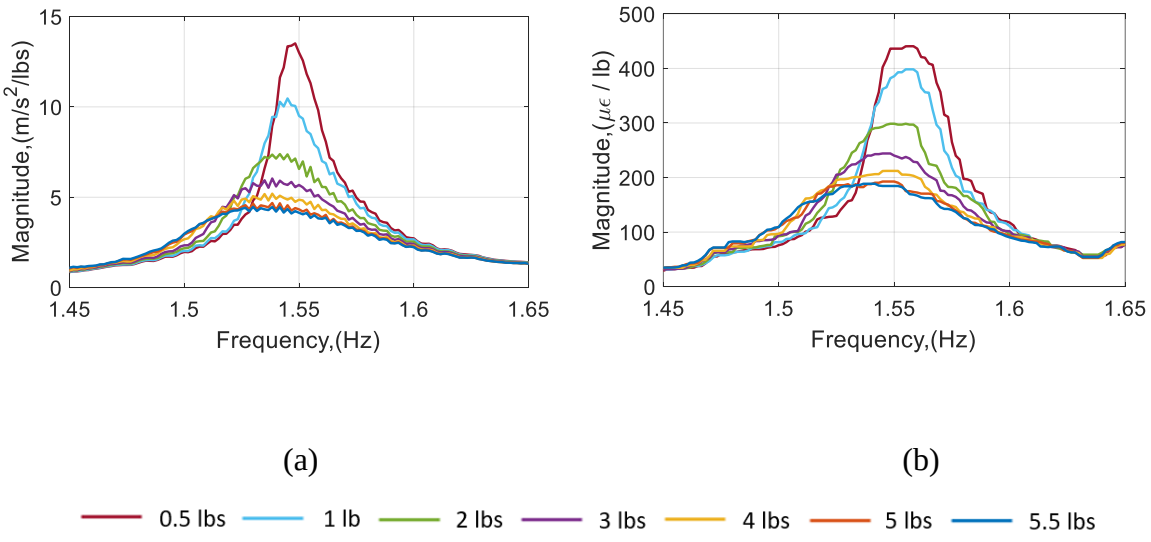

Figure 25 Frequency response function from accelerometer (a) and LEWIS-S (b)

As is often the case for analysis of dynamical systems, the use of transfer functions is useful to map the response amplitudes at a prescribed load level. From the measured data, both acceleration and strain provide different curves in the vicinity of the resonant peak, and generally overlay away from the resonance. This distortion of the FRF near resonance is classical nonlinear behavior, and thus can provide significant insights into the dynamics of the system. For example, one could assume that the low-level test at 0.5 lbs would be a valid approximation to the linear system. Without testing explicitly at higher levels, the linear FRF from test would provide the mapping between strain at resonance and the force level. Assuming the peak strain at 1.55 Hz is approximately 450 με/lb, an approximation to the strain at resonance for the 5.5 lb test would be $2.48 \cdot 10^3$ με. Reverting back to the direct strain measurements in Figure 25, the peak strain was significantly less at a value of $1.14 \cdot 10^3$ με. Obtaining these direct measurements of strain enables experiments at higher levels to validate the use of linear theory and understand when nonlinearity can influence the estimates of strain levels during test.

The CWT is a conventional method for analyzing nonlinear responses which is generally more advantageous than Fourier Transforms or Short Time Fourier Transforms [47]. That is, the CWT analyzes the amplitude-time-frequency content of a nonstationary signal such that a moving window captures the evolution of the signal [48, 49]. The CWT's of the accelerometer and LEWIS-S from the sine sweeps were plotted in Figure 26.

The frequencies of the responses were analyzed as functions of time where the changes in the normalized amplitude content of the signal can be seen. When the beam is in the linear regime at low forces and small displacements the peak amplitudes appear localized. Conversely, when the beam is subjected to larger forces and resultingly large displacements,

the peak amplitudes in the CWT's start to shift and span over longer time intervals. This comparison can be seen between the lowest and highest forcing excitation in Figure 26. The nonlinear response shifts the frequency such that the peak amplitudes occur approximately a minute, or 0.02 Hz before the peak amplitudes in the lowest force and retain larger magnitudes with respect to time. Lastly, it is noted that no higher harmonics were found in the CWT analysis for the large forcing amplitude responses.

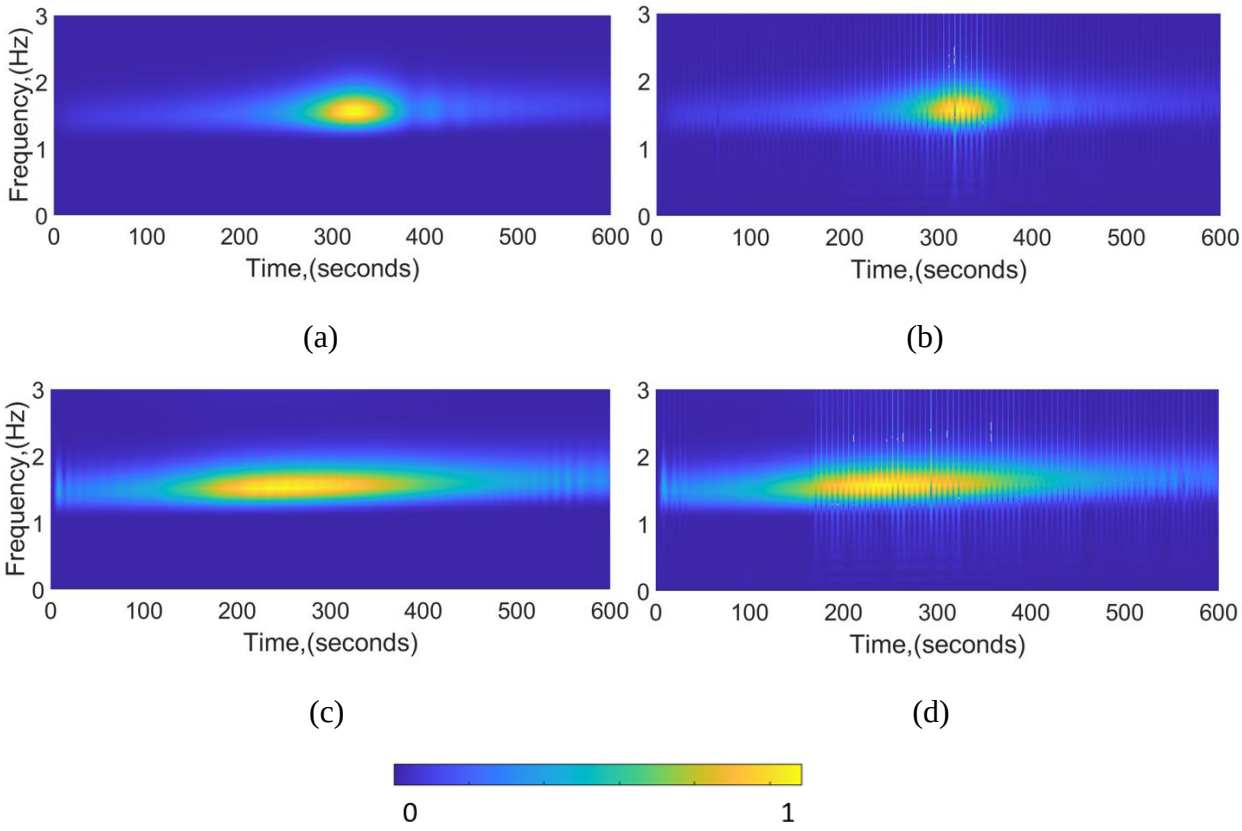

Figure 26 Continuous wavelet transforms of accelerometer responses at 0.5 lbs (a) and 5.5 lbs (c) and strain gauge responses at 0.5 lbs (b) and 5.5 lbs (d) from sine sweep tests

4.5 Nonlinear Ring-down Testing

A series of nonlinear ring-down experiments were performed by applying an initial large displacement to the tip of the beam and releasing from the static equilibrium. The ring-down response was measured using both the accelerometer and LEWIS-S for a period of 90 seconds. From the measured data, the frequency backbone curves could be estimated from the time histories using the zero-crossing method in [50]. The initial static deformation of the beam is approximately that of the first bending mode, however transients were observed in the initial portion of the ring-down, as shown in Figure 27.

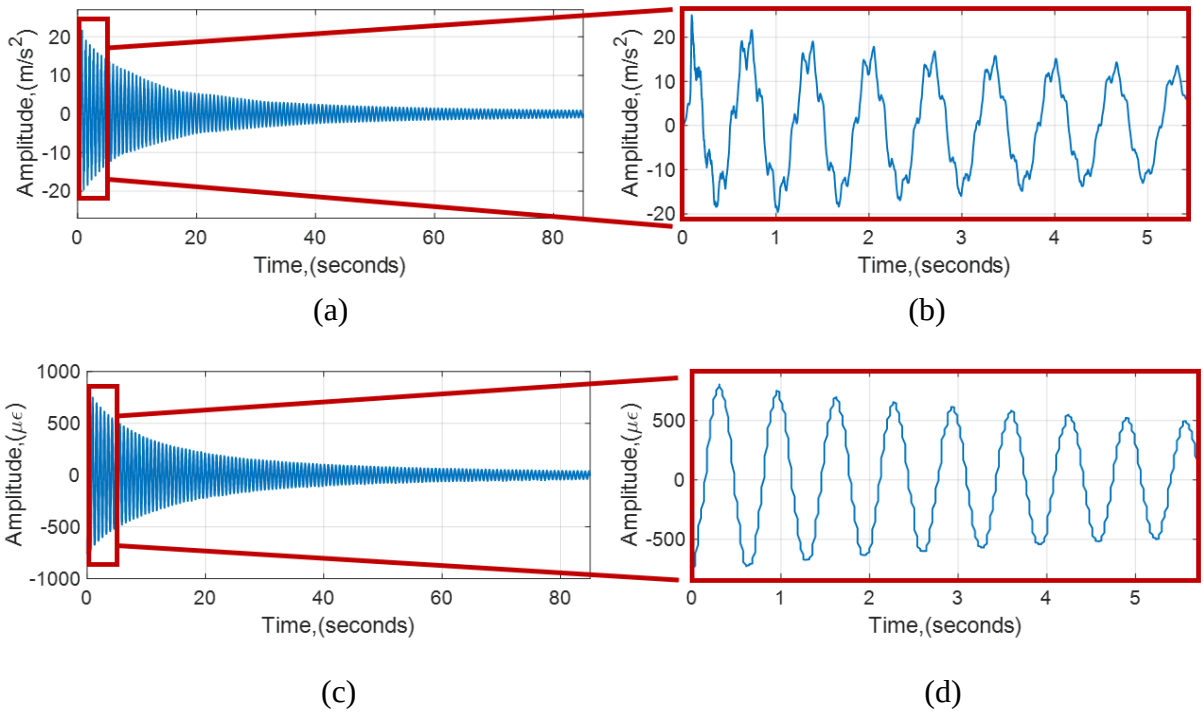

Figure 27 Accelerometer and strain time history of ring-down test (a),(c), initial 5-second segments that demonstrate transients in the response (b),(d)

In order to isolate a monoharmonic response for the zero-crossing method, the transient response had a bandpass filter applied from 1 Hz to 3 Hz to determine the time-frequency and backbone curves. The bandpass filter also made the signal of the ring-down time-histories cleaner for the zero-crossing method. In addition to the bandpass filter, data after the first three cycles (approximately 2 seconds) of the ring-down time histories were used to assure transients decayed out leaving predominantly single-mode responses.

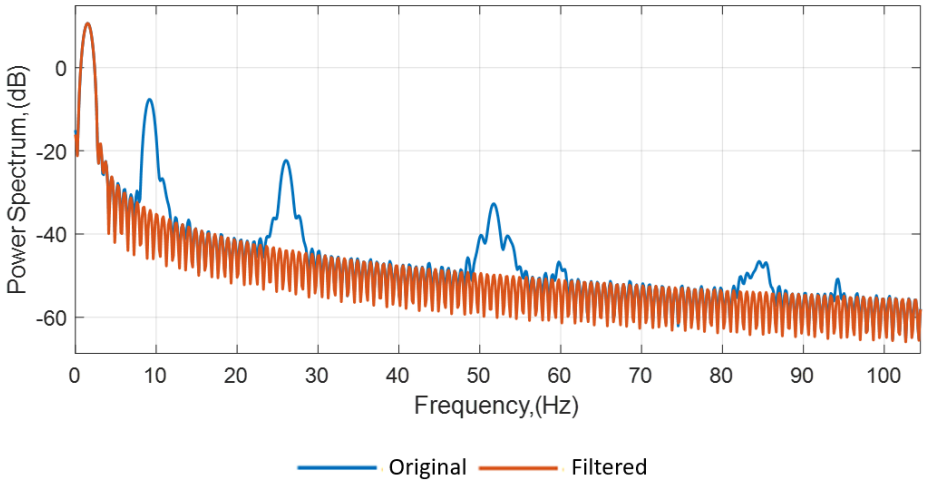

Figure 28 Power spectrum of filter used in ring-down tests

Following the bandpass filtering, the time histories are processed using the zero-crossing method in [50]. Figure 27 shows the amplitude-dependent backbone curves for the first mode from the ring-down acceleration and strain measurements. Three separate tests were conducted, each with approximately the same initial static displacements, in order to observe and verify the repeatability of the tests. In addition to using a bandpass filter, the accelerometer and LEWIS-S results were both filtered using Savitzky-Golay filters that utilized the same

frame lengths and weights in order to reduce noise. The backbone curves in Figure 27 show good qualitative agreement between the strain and acceleration response, verifying the ability of the LEWIS-S to effectively measured the softening in the beam. Additionally, the ring-down response verifies the softening behavior, and hence inertia nonlinearity dominated response, of the cantilever beam. This data shows the versatility of the types of experiments that can be conducted with the LEWIS-S to characterize and identify nonlinearity in a structure.

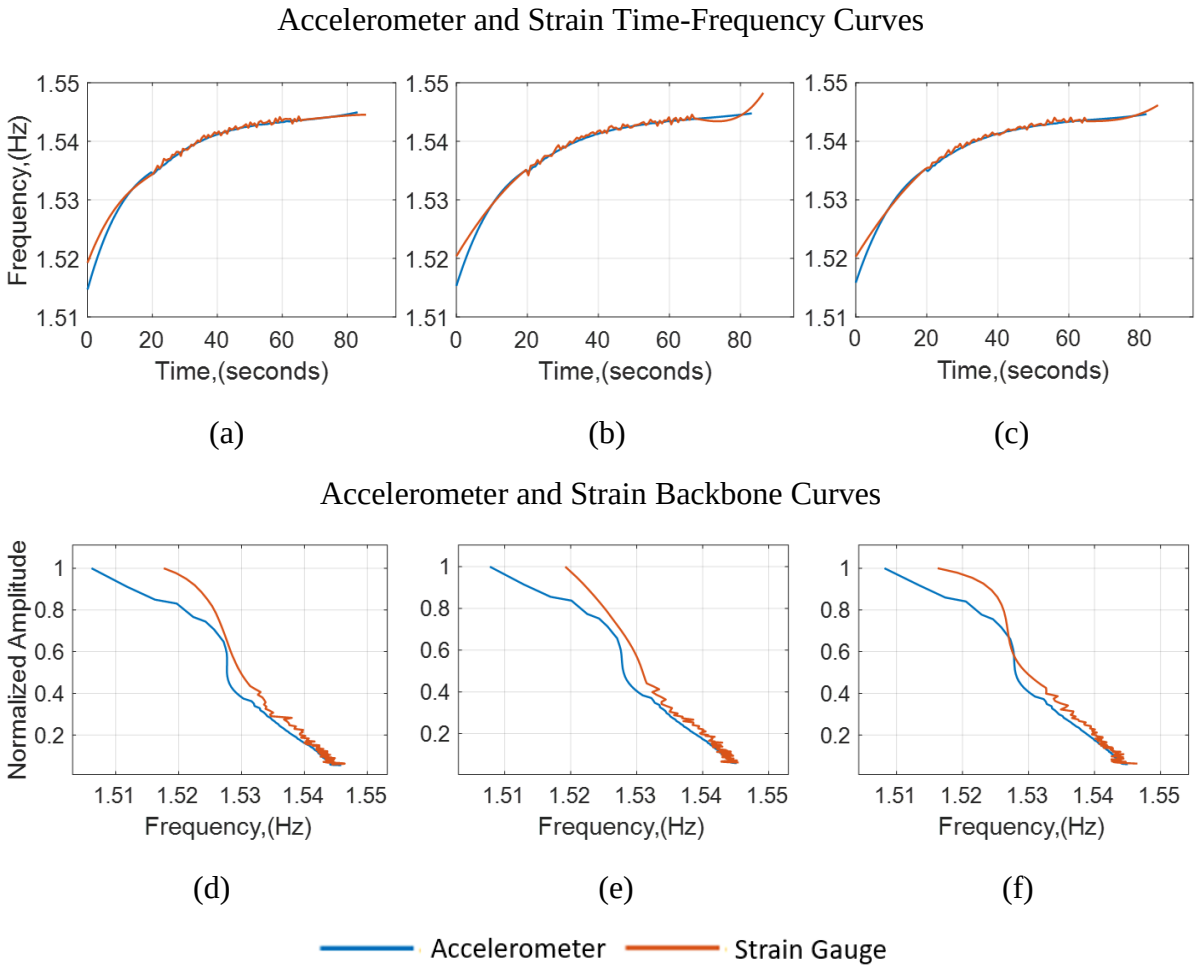

Figure 29 Accelerometer and strain time-frequency curves test 1 (a),test 2 (b), test 3(c) and accelerometer and strain backbone curves test1 (d), test 2 (e), test 3 (f)

4.6 Conclusions

Based on the results from the series of sine sweeps and ring-down tests, the LEWIS-S sensor demonstrated identical results to those obtained by the accelerometer. The softening behavior caused by the nonlinearity in the cantilever beam was accurately characterized by the LEWIS-S in comparison to the accelerometer responses. This suggests that the LEWIS-S can be a viable sensing alternative to accelerometers for inertia and geometric nonlinear characterization in vibration testing. Furthermore, the LEWIS-S streamlines the strain sensing by introducing a low-cost and portable design platform.

Chapter 5 Conclusions and Future Research

5.1 Summary

This thesis introduces the design and development of a low-cost, efficient wireless intelligent sensor for strain measurements (LEWIS-S). The LEWIS-S is a low-cost strain gauge sensor that is compact and versatile which introduces significant benefits over large and costly commercial DAQ equipment. The LEWIS-S sensor introduces the benefit of retaining a simple design such that researchers with limited knowledge on sensing technologies could assemble and use the sensor in a short period of time. Additionally, the versatility of the LEWIS-S sensor introduces the capability of accepting different types of strain gauge attachments that allows for the option of traditional or quick strain sensing.

Researchers validated the function of the sensor by performing static and dynamic laboratory testing where the accuracy and overall effectiveness of the LEWIS-S was demonstrated and quantified. The static and dynamic testing on the cantilever beam demonstrated that the two LEWIS-S configurations retained good accuracy and comparable results to that of the expensive commercial DAQ system. Although the LEWIS-S1 consistently retained lower signal to noise ratios and contained some drift, the experimental tests demonstrated that different strain gauge attachments are accurate and viable low-cost solutions to measuring strain. Based on the results obtained from the validation testing of the LEWIS-S, future work regarding sensor enhancements will include the implementation of different ADC amplifiers to increase the sampling rates, the design of a robust Wheatstone bridge to mitigate noise and drift, and to perform field-testing validation experiments. This will be discussed in greater detail in the proceeding sections.

Furthermore, it was also demonstrated that the lumped mass and wiring from the accelerometer can significantly affect the dynamics of the system such that the errors between the resonant frequencies and damping coefficients were 10% and 33%, respectively. A set of sine sweep tests were conducted on the beam where the nonlinear responses were characterized by computing the FRF which demonstrated softening effects. The CWT was also computed for both sensor responses where no higher harmonics were found but it was confirmed that the same softening effects were observed. Lastly, ring-down tests were conducted to obtain the time-frequency and backbone curves of the beam where a consistent and clear softening effect was again observed. The results between the accelerometer and LEWIS-S demonstrated good agreement and additionally demonstrated repeatable results. Based on the results from the forced vibration and ring-down testing, the LEWIS-S and accelerometer showed similar behaviors from the both analyses suggesting the LEWIS-S can be an effective method to characterize inertial and geometric nonlinearities on a cantilever beam.

5.2 Limitations

One of the biggest limitations on the LEWIS-S that resulted in minor setbacks were the two potentiometers on the Wheatstone bridge on the LEWIS-S1 sensor configuration. Generally, after the sensor is powered on for the first time, the two potentiometers in the Wheatstone bridge require adjustment until the ADC values read approximately 8,400,000 bits, or something near this value as this was half the resolution of the ADC. Additionally, the bridge required some time to equilibrate after adjustment of the potentiometers. As seen from the experimental testing, it is sometimes possible for the sensor to drift if it is not fully equilibrated.

A cost effective and straightforward fix would be to modify the external Wheatstone bridge with new resistors so the ADC would reach and maintain half resolution upon initial start-up.

Throughout the laboratory experimentation and validation testing, the analog-to-digital converter on the LEWIS-S limited the sensor to a sampling rate of 80-90 Hz. Although this sampling rate may be permissible in some research and applications, it can be limiting for higher frequency testing. However, in order to address the restricted sampling rate on the LEWIS-S a new ADC could be installed such that the sampling rate is increased, and the low cost of the sensor is maintained.

Furthermore, the real time clock (RTC) on the Arduino Uno demonstrated some limitations during post-processing. Generally, the RTC on the Arduino Uno had an inconsistent time step so data would resultingly retain an inconsistent sampling rate. Therefore, data-interpolation was required to process results after experiments. Similar to the ADC on the LEWIS-S, an external RTC can be added to the sensor so the time steps maintain constant intervals. Despite, these two limitations on the LEWIS-S, the Arduino platform demonstrates significant versatility as there are a broad range of cost-effective sensor and chip components available in the market that offer different specifications.

5.3 Future Research and Applications

The following section will present the future research of the LEWIS-S where collaborations and further sensor development will be discussed. The future research of the LEWIS-S sensor introduces and highlights the application of more laboratory testing and field testing where findings can be investigated and implemented into future generations of the sensor.

5.3.1 Strain Sensing on Amateur High-Altitude Model Rockets

The Smart Management of Infrastructure Laboratory (SMILab) has been in close collaboration with the Albuquerque Rocket Society (ARS) for applying sensors and monitoring acceleration and strain during high altitude model rocket flights. The future work of the LEWIS-S includes deployment on a high-altitude amateur model rocket to collect strain data on the base of the fin. Vibration data of interest includes determining nonlinear responses of the wing during flight and damage detection. The future work of strain sensing on the high-altitude model rockets introduces unique sensing opportunities due to various reasons: firstly, rocket sensing requires reliable wireless sensing, secondly, it requires a robust, portable design as sensor placement within the rocket body is very restrictive, and lastly, the sensing environment within the rocket body proves to be a harsh environment for the sensor so a durable design is required.

Figure 30 High-Altitude amateur model rockets from the Albuquerque Rocket Society and the LEWIS-S sensor

5.3.2 Solar Powered Design

Since the LEWIS-S has a relatively low power consumption, future research in a solar powered design is being considered for the next generation sensor. Researchers at SMILab have developed solar powered sensors for the original LEWIS sensor where a small incasement provides solar power and a weatherproofing. The future research directed to the design of a solar powered LEWIS-S sensor will provide a solution for long-term deployments on infrastructure and structural applications such as bridges or the Tram towers located in Albuquerque, NM where the first solar powered LEWIS sensor was deployed. Long term strain sensing would give the LEWIS-S sensor greater capabilities in both static and dynamic environments in the field.

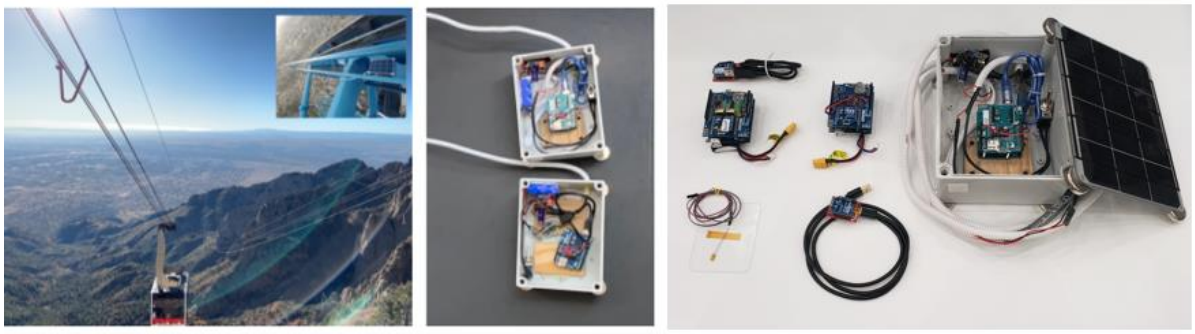

Figure 31 LEWIS-S sensor, LEWIS sensor, and solar powered LEWIS sensor

5.3.3 Experimental Large Forced Vibrations

Future laboratory research that utilizes the LEWIS-S sensor that is under consideration is the application of large excitation forcing for dynamic testing. Testing with large excitation forcing is useful in damage detection and nonlinear dynamics with large excitations. Additionally, nonlinear control based on strain measurements will be considered during large forcing excitations with the LEWIS-S sensor. This future testing will reveal new findings and capabilities that will enhance future designs of the LEWIS-S sensor.

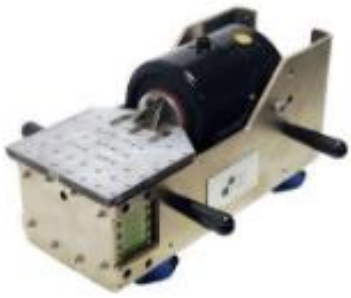

Figure 32 Large vibration shaker with horizontal flexure table [51]

5.4 Publications Related to this MS Thesis Document

- Robbins, E., Cobo, N., Diaz, J., Moreu, F. "Development of a Low-Cost Efficient Wireless Intelligent Sensor for Strain Measurements (LEWIS-S)." *Measurement Science and Technology*, 2021, doi:10.1088/1361-6501/abe339. https://iopscience.iop.org/article/10.1088/1361-6501/abe339/pdf (Chapter 3 of this thesis)

- Robbins, E., Kuether, R., Moreu, F. “Measuring Large Deformations of a Cantilever Beam Using a Low-Cost Efficient Wireless Intelligent Sensor for Strain (LEWIS-S).” *Measurement Science and Technology*, 2021.

  (Chapter 4 of this thesis, to be submitted in May 2021)

References

[1] Ewins, D. J. Modal Testing: Theory, Practice and Application. Research Studies Press, 2000.

[2] Worden, K., and Geoffrey R. Tomlinson. Nonlinearity in Structural Dynamics: Detection, Identification, and Modelling. Institute of Physics, 2001.

[3] D.J. Ewins, B. Weekes, A. Delli CarriModal testing for model validation of structures with discrete nonlinearities. Philos. Trans. R. Soc. A, 373 (2015), p. 20140410

[4] A.F. Vakakis, L.I. Manevitch, Y.V. Mikhlin, V.N. Pilipchuk, A.A. Zevin, Normal Modes and Localization in Nonlinear Systems, Wiley Series in Nonlinear Science, John Wiley & Sons, New York, 1996.

[5] Graspengineering, What Is Nonlinear Analysis ? Types of Nonlinearity, 14 Sept. 2020, www.graspengineering.com/what-is-nonlinear-analysis-types-of-nonlinearity/

[6] Beigelbeck, R., Antlinger, H., Cerimovic, S., Clara, S., Keplinger, F., and Jakoby, B. Published 22 October 2013. Resonant pressure wave setup for simultaneous sensing of longitudinal viscosity and sound velocity of liquids. Measurement Science and Technology, Volume 24, Number 12. 2013 IOP Publishing Ltd. https://iopscience.iop.org/article/10.1088/0957-0233/24/12/125101/meta

[7] N J Lawson, R Correia, S W James, M Partridge, S E Staines, J E Gautrey, K P Garry, J C Holt and R P Tatam. Published 16 September 2016. Development and application of optical fiber strain and pressure sensors for in-flight measurements. Measurement Science and Technology, Volume 27, Number 10. 2016 IOP Publishing Ltd. https://iopscience.iop.org/article/10.1088/0957-0233/27/10/104001

[8] Chandran, P., Rantatalo, M., Odelius, J., Lind, H., and Famurewa, S. Published 19 September 2019. Train-based differential eddy current sensor system for rail fastener

detection. Measurement Science and Technology, Volume 30, Number 12. 2019 IOP Publishing Ltd. https://iopscience.iop.org/article/10.1088/1361-6501/ab2b24

[9] Huang, D., Liu, H., Zhu, L., Li, M., Xia, X., and Qi, J. Published 17 December 2020. Soil organic matter determination based on artificial olfactory system and PLSR-BPNN. Measurement Science and Technology, Volume 32, Number 3. 2020 IOP Publishing Ltd. https://iopscience.iop.org/article/10.1088/1361-6501/abc964/meta

[10] American Society of Civil Engineers, 2021, Infrastructure Report Card https://infrastructurereportcard.org/infrastructure-categories/

[11] (n.d.). Structural Health Monitoring - IIT Kanpur. Retrieved September 24, 2020, from http://www.iitk.ac.in/ce/test/MoHUPA%20Presentation_Dr.K%20Roy%20_%20Dr.S.Mukhopadhya.pdf

[12] Instron - USA. (2019, October 25). The Importance of Strain Measurement in Materials Development. AZoM. Retrieved on September 24, 2020 from https://www.azom.com/article.aspx?ArticleID=12521.

[13] (n.d.). Stress & Strain - NDT Resource Center. Retrieved September 24, 2020, from https://www.nde-ed.org/EducationResources/CommunityCollege/Materials/Mechanical/StressStrain.htm

[14] ASTM E251-20a, Standard Test Methods for Performance Characteristics of Metallic Bonded Resistance Strain Gages, ASTM International, West Conshohocken, PA, 2020, www.astm.org

[15] D. Dias-da-Costa, Jónatas Valença, Eduardo N.B.S. Júlio, Laboratorial test monitoring applying photogrammetric post-processing procedures to surface displacements, Measurement, Volume 44, Issue 3, 2011, Pages 527-538, ISSN 0263-2241, https://doi.org/10.1016/j.measurement.2010.11.014. (http://www.sciencedirect.com/science/article/pii/S0263224110003040)

[16] Marques dos Santos, Fabio & Peeters, Bart & Lau, Jenny & Desmet, Wim & Goes, Luiz. (2014). An overview of experimental strain-based modal analysis methods.

[17] Baharin, Hatini & Rahman, Roslan. (2009). Effect of accelerometer mass on thin plate vibration. J Mek. 29.

[18] D. Rovˇsˇcek, J. Slaviˇc and M. Bolteˇzar. The use of strain sensors in an experimental modal analysis of small and light structures with free-free boundary conditions. Journal of Vibration and Control, 2013, Volume 19, Issue 7, May 2013, Pages 1072-1079. DOI: 10.1177/1077546312445058

[19] Marques dos Santos, Fabio & Peeters, Bart. (2016). On the use of strain sensor technologies for strain modal analysis: Case studies in aeronautical applications. Review of Scientific Instruments. 87. 102506. 10.1063/1.4965814.

[20] Jiang X, Li B, Mao X, Peng Y, He S. New approach based on operational strain modal analysis to identify dynamical properties of the high-speed reciprocating operation mechanism. Journal of Low Frequency Noise, Vibration and Active Control. 2019;38(3-4):1345-1362. doi:10.1177/1461348418821203

[21] N. Tourjansky and E. Szechenyi, The measurement of blade deflections-a new implementation of the strain pattern analysis, ONERA Technical Paper 1 (1992).

[22] Luis, Fabio & Marques dos Santos, Fabio & Peeters, Bart & Lau, Jenny & Desmet, Wim & Luiz, Carlos & Goes, Luiz. (2015). The use of strain gauges in vibration-based damage detection. Journal of Physics: Conference Series. 628. 10.1088/1742-6596/628/1/012119.

[23] Santos, F.L., Peeters, B., Debille, J., Salzano, C., Góes, L.S., & Desmet, W. (2015). The Use of Dynamic Strain Sensors and Measurements on the Ground Vibration Testing of an F-16 Aircraft.

[24] H. Wentzel, Fatigue test load identification using weighted modal filtering based on stress, Mechanical Systems and Signal Processing 40 (2013), 618–627. 2466 PROCEEDINGS OF ISMA2014 INCLUDING USD2014

[25] L. H. Yam, D. B. Li, T. P. Leung, and K. Z. Xue, Experimental study on modal strain analysis of rectangular thin plates with small holes, Pro

[26] Malatkar, Pramod. (2003). Nonlinear Vibrations of Cantilever Beams and Plates. Dissertation. Virginia Polytechnic Institute and State University.

[27] Delgado-Velázquez, Iván, "Nonlinear vibration of a cantilever beam" (2007). Thesis. Rochester Institute of Technology.

[28] Robert M. Jones and Harold S. Morgan. Analysis of Nonlinear Stress-Strain Behavior of Fiber-Reinforced Composite Materials. AIAA Journal 1977 15:12, 1669-1676

[29] Yao, H., Cao, H., & Li, J. (2016). Design and Implementation of a Portable Wireless System for Structural Health Monitoring. Measurement and Control, 49(1), 23–32. https://doi.org/10.1177/0020294015615895

[30] Chacón, R., Guzmán, F., Mirambell, E., Real, E., & Oñate, E. (2009). Wireless Sensor Networks for Strain Monitoring during Steel Bridges Launching. Structural Health Monitoring, 8(3), 195–205. https://doi.org/10.1177/1475921708100779

[31] Jo, Hongki & Park, Jongwoong & Spencer, Billie & Jung, Hyung-Jo. (2012). Design and validation of high-precision wireless strain sensors for structural health monitoring of steel structures. Proceedings of SPIE - The International Society for Optical Engineering. 8345. 29-. 10.1117/12.915392.

[32] Amedeo Gregori,[1] Emidio Di Giampaolo,[2] Alessandro Di Carlofelice,[2] and Chiara Castoro (2019) Presenting a New Wireless Strain Method for Structural Monitoring: Experimental Validation
https://doi.org/10.1155/2019/5370838

[33] Abdulkarem, Mohammed & Samsudin, Khairulmizam & Rokhani, F.Z. & Rasid, Mohd. (2019). Wireless sensor network for structural health monitoring: A contemporary review of technologies, challenges, and future direction. Structural Health Monitoring. 147592171985452. 10.1177/1475921719854528.

[34] Lynch, Jerome & Loh, Kenneth. (2006). A Summary Review of Wireless Sensors and Sensor Networks for Structural Health Monitoring. The Shock and Vibration Digest. 38. 91-128. 10.1177/0583102406061499.

[35] N.C. Yoder, D.E. Adams, 3 - Commonly used sensors for civil infrastructures and their associated algorithms, In Woodhead Publishing Series in Electronic and Optical Materials,Sensor Technologies for Civil Infrastructures, Woodhead Publishing, Volume 55, 2014, Pages 57-85, ISBN 9780857094322,
(http://www.sciencedirect.com/science/article/pii/B9780857094322500036)

[36] Peter A. Claisse, Chapter 2 - Strength of materials, Editor(s): Peter A. Claisse, Civil Engineering Materials, Butterworth-Heinemann, 2016, Pages 9-22, ISBN 9780081002759, https://doi.org/10.1016/B978-0-08-100275-9.00002-4.
(http://www.sciencedirect.com/science/article/pii/B9780081002759000024)

[37] (n.d.). Arduino Official Store - Arduino Uno Rev3 Technical Specificaions. Retrieved September 24, 2020, from https://store.arduino.cc/usa/arduino-uno-rev3

[38] #133943, Member, et al. “SparkFun Load Cell Amplifier - HX711.” PDF datasheet file. SEN-13879 - SparkFun Electronics, https://www.sparkfun.com/products/13879.https://cdn.sparkfun.com/datasheets/Sensors/ForceFlex/hx711_english.pdf

[39] “XBee/XBee-PRO S2C 802.15.4 Radio Frequency (RF) Module User Guide.” PDF file. DigiKey, Digi, https://www.digikey.com/product-detail/en/digi-international/XB24CDMWIT-001/602-1967-ND/6226955&?gclid=Cj0KCQjwyLDpBRCxARIsAEENsrKjcFdTEZh0FjWfEKw5S_Ecpy6vhkrGBl8RgfLKbeEYOM8DquQ-ZeYaAsqEEALw_wcB.

[40] Maurer, Matt. SparkFun XBee Explorer USB. https://www.sparkfun.com/products/11812.

[41] Hoffmann, K.: An Introduction to Measurements using Strain Gages. Hottinger Baldwin Messtechnik GmbH, Darmstadt (1989)

[42] (n.d.). Shunt Calibration of Strain Gage Instrumentation, Vishay Precision Group, Micro-Measurements, from http://www.vishaypg.com/docs/11064/tn514.pdf

[43] Series Y Strain Gages (SG) Datasheet. PDF file. HBM, https://www.hbm.com/fileadmin/mediapool/hbmdoc/temporary-shop-files/b4709.pdf.

[44] (n.d.). Frictional Strain Checker FGMH Series, Tokyo Measuring Instruments Laboratory, from https://tml.jp/eng/documents/strain_gauge/StrainChecker_FGMH.pdf

[45] Malatkar, P. (2003) Nonlinear Vibrations of Cantilever Beams and Plates (Doctoral Dissertation, Virginia Polytechnic Institute and State University, Blacksburg, Virginia)

[46] Sracic, Michael & Yang, Shifei & Allen, Mathew. (2012). Comparing Measured and Computed Nonlinear Frequency Responses to Calibrate Nonlinear System Models. Conference Proceedings of the Society for Experimental Mechanics Series. 3. 255-267. 10.1007/978-1-4614-2416-1_21.

[47] M. Peeters, G. Kerschen, J.C. Golinval, Dynamic testing of nonlinear vibrating structures using nonlinear normal modes, Journal of Sound and Vibration, Volume 330, Issue 3, 2011, Pages 486-509, ISSN 0022-460X

[48] S. Mallat, A Wavelet Tour of Signal Processing, second ed., Academic Press, London, 1999.

[49] Addison, Paul S., Introduction to redundancy rules: the continuous wavelet transform comes of age, Philosophical Transactions of the Royal Society A: Mathematical, Physical and Engineering Sciences, 10.1098/rsta.2017.0258.

[50] Julián M. Londoño, Simon A. Neild, Jonathan E. Cooper, Identification of backbone curves of nonlinear systems from resonance decay responses, Journal of Sound and Vibration, Volume 348,2015,Pages 224-238,ISSN 0022-460X

[51] “Vibration Shaker Horizontal Table.” Vibration Shaker Horizontal Table | Excitation | The modal Shop, Inc., www.modalshop.com/excitation/excitation.asp?ID=580.